Environmental Conditions Associated with Long-Track Tornadoes

JERRY M. STRAKA,[a] VITTORIO A. GENSINI,[b] KATHARINE M. KANAK,[c] AND JONATHAN M. GARNER[d]

[a] *University of Oklahoma, Norman, Oklahoma*
[b] *Northern Illinois University, DeKalb, Illinois*
[c] *Independent Scientist, Norman, Oklahoma*
[d] *Independent Scientist, Fort Wayne, Indiana*

(Manuscript received 9 February 2024, in final form 26 August 2024, accepted 29 August 2024)

ABSTRACT: Reanalysis proximity vertical profile attributes associated with long-track tornadoes [LTTs; pathlength ≥ 48 km (30 mi)] and short-track tornadoes [STTs; pathlengths < 48 km (30 mi)] for a total of 48 212 tornadoes with pathlengths ≥ 0.016 km (0.01 mi) from 1979 to 2022 in the United States were examined. Both longer- and shorter-track tornadoes were associated with vast ranges of mixed-layer convective available potential energy, together with relatively low mixed-layer lifted condensation level heights and minimal convective inhibition. A large range of 500–9000-m wind speeds and bulk wind differences, 500–3000-m streamwise vorticities, storm-relative helicities, and storm-relative wind speeds were found for STTs. In stark contrast, LTTs only occurred when these kinematic attributes were larger in amplitude through the troposphere, supporting previously documented associations between observed longer-track tornado pathlengths and faster-propagating parent storms. A novel parameter, heavily weighted by kinematic parameters and lightly weighted by thermodynamic parameters, outperformed the significant tornado parameter in differentiating environments that were more supportive of both LTTs and tornadoes rated <EF5. The high correlation values $R^2 = 0.79$ between tornado pathlength and Bunkers' approximate tornado duration (pathlength/V_{Bunkers}) call for improved understanding of mesocyclone periodicities, which impact tornado longevity, to improve tornado pathlength diagnoses and forecasts. Pragmatically, diagnosing LTT environments using vertical profile attributes, perhaps, is not so much a problem of determining when there might be higher expectations for LTTs, but rather a problem of when there might be lower expectations for LTTs, e.g., weaker kinematic attributes in the lower troposphere.

SIGNIFICANCE STATEMENT: The majority of tornadoes have pathlengths less than a few kilometers. As tornado pathlengths increase, their probability of causing impacts to society also increases. We study >40 years of modeled atmospheric vertical profiles to better understand the environmental conditions that support long-track tornadoes (pathlength ≥ 48 km or ≥30 mi). Consistent with previous studies, long-track tornadoes occurred with substantially stronger vertical wind shear profiles and low-level winds compared to short-track tornadoes; however, most tornadoes did not form in environments with exceedingly large vertical instability, regardless of pathlength or intensity. A proposed composite long-track tornado parameter (LTTP) provided better discrimination between longer and shorter pathlength events compared to preexisting parameters.

KEYWORDS: Tornadoes; Convective storms; Storm environments; Reanalysis data

1. Introduction

Long-track tornadoes [LTTs; pathlengths[1] (PLs) ≥ 30 mi or ≥48 km based on Straka and Kanak 2022, hereafter SK22] have a greater propensity to cause significant societal impacts (e.g., Grieser and Terenzi 2016). In general, longer-track tornadoes cause more property loss, injuries, and deaths per path mile compared to tornadoes with pathlengths < 30 mi (Kelly et al. 1978; SK22). These increased impacts stem from longer tornado durations, larger tornado areal footprints, generally wider tornado paths, the potential to impact more damage indicators, and the tendency for LTTs to produce higher E(F)-scale rated damage (SK22).

The elementary mechanism that permits a tornado to be long track (versus a relatively shorter track) could be thought of, at least in part, as a simple advective time-scale problem. That is, tornado-producing convective storms (e.g., supercells) will result in greater pathlengths with increasing storm motion velocity (all else being equal). However, even with similar storm motions, tornado pathlengths can vary significantly due to factors impacting updraft strength, near-surface streamwise vorticity, tornado location (and location change) under the updraft (Dowell and Bluestein 2002; Marquis et al. 2012), low-level mesocyclone occlusion frequency (Adlerman et al. 1999), spatiotemporal evolution of the near-storm environment, and a plethora of other factors. This makes diagnosing environments favorable for LTTs particularly difficult and further complicated by the additional challenge of anticipating when/if near-future environments may be more or less favorable for LTT

[1] Hereafter, we only use units in miles (yards) for pathlengths (pathwidths) as reported in the Storm Prediction Center dataset.

Supplemental information related to this paper is available at the Journals Online website: https://doi.org/10.1175/WAF-D-24-0021.s1.

Corresponding author: Jerry M. Straka, jerrystraka@gmail.com

DOI: 10.1175/WAF-D-24-0021.1

events. Part of this challenge stems from the relative rarity of tornado events (compared to supercells) overall, especially LTTs (<1% of all tornadoes; SK22).

The objectives of this work were to identify important environmental characteristics associated with LTTs, as well as to explore the feasibility of creating a statistically robust long-track tornado parameter. As is common with other severe convective storm composite parameters, there is not likely to be a "magic bullet" parameter that will provide perfect environmental discrimination (Doswell and Schultz 2006). Rather, our goal was to develop a composite parameter that could aid forecasters in diagnosing which atmospheric environments are potentially supportive of LTT events or, conversely, which environments are potentially not supportive of LTT events. We approached this issue by examining over 200 variables, derived indices, and composite parameters from reanalysis vertical profiles located in close spatial and temporal proximity to 48 212 tornadoes in the United States over a period of 44 years (1979–2022).

2. Background

For decades, data from observed soundings have been an essential source of information to better understand environmental features associated with tornadoes (e.g., Beebe 1958; Darkow 1969; Kelly et al. 1978; Schaefer and Livingston 1988; Parker 2014). However, operational radiosonde launches rarely occur in the vicinity of a tornado, and obtaining them in field-based research settings is challenging, often resulting in limited cases and very restricted population sizes. To augment population sizes, several studies have used model-derived vertical profiles to serve as synthetic proximity soundings (Thompson et al. 2003, hereafter T03; Taszarek et al. 2020b, hereafter T20b; Gensini et al. 2021; Garner et al. 2021, hereafter G21). In conjunction with independent modeling efforts, these works helped to conclude that, for tornadoes, sufficient 0–6-km wind shear, low heights of lifting condensation level (LCL), adequate near-surface storm-relative helicity (SRH), and low static stability were fundamental ingredients. Synthetic proximity soundings are not perfect and can be subject to limitations due to horizontal and vertical resolution and choice of model parameterization schemes (Brooks et al. 2003; Gensini and Ashley 2011; Coniglio 2012; Gensini et al. 2014; King and Kennedy 2019; Coniglio and Jewell 2022). There are also important considerations regarding the spatial and temporal criteria used to classify the model vertical profiles as proximity soundings (Potvin et al. 2010).

In research closely related to this study, the significant tornado parameter (STP) was derived using Rapid Update Cycle-2 (RUC-2) model proximity soundings in the vicinity of supercell and isolated nonsupercell storms (T03). Key factors, including pronounced 0–6-km vertical wind shear, 0–1-km SRH, 0–1-km relative humidity, convective available potential energy (CAPE), and relatively low above-ground-level (AGL) mixed-layer LCL heights, were effective in distinguishing between tornadic and nontornadic supercells. A later extension of this research introduced SRH within an effective inflow layer (ESRH; Thompson et al. 2007, hereafter T07) and the effective bulk wind difference (EBWD). More recent studies suggest that refining the integration layers for SRH, such as using 10–500 or 10–100 m (Coffer et al. 2019, hereafter C19; Coffer et al. 2020), can improve STP's discriminating capabilities using STP with 10–1000 m or ESRH for EF2+ rated tornadoes. Stronger ground-relative winds associated with certain storm motions also can result in conditions more conducive to significant tornadoes (Coniglio and Parker 2020).

Prominent signals for significant tornadoes including large CAPE, low LCL height, large low-level shear and SRH, along with strong surface to 6000-m bulk shear or velocity difference, are also important for longer-track tornadoes. However, LTTs also are associated with environments with stronger winds in the middle- (e.g., 3000–5000 m) and upper-level (e.g, 7000–10 000 m) winds, 10–8000-m bulk wind difference (Garner 2007, hereafter G07) or effective bulk wind difference (EBWD; G21), which is consistent with Bunkers et al. (2006, hereafter B06) and Davenport (2021) in their research on long- and very-long-lived supercells. Also, faster mean tropospheric winds generally lead to faster storm motions (Bunkers et al. 2000, 2014). Crucially, SK22 suggested that longer-track tornadoes required longer-lived parent supercells with noncyclic or weakly cyclic mesocyclones and that tornado durations were limited, at least in part, by the period of cyclicity of mesocyclones; thus, weakly and noncyclic mesocyclones are more likely to produce LTTs. Little else concerning environmental conditions specifically related to longer-track tornadoes has been documented in scientific literature to date. With this, and the fact that previous studies used limited (by availability in both time and space) observed rawinsonde data for LTTs, the primary motivation for the work herein is to build on these previous studies by exploring background environmental states that may successfully aid in the statistical discrimination of LTT events (effectively all reported LTT events) for a larger population size of LTTs from 1979 to 2022 using synthetic reanalysis proximity soundings.

3. Data and methods

a. Tornado report data

Tornado report data, including pathlength, from 1979 to 2022 were obtained from the Storm Prediction Center public web page at https://www.spc.noaa.gov/wcm/ (Schaefer and Edwards 1999). Though these reports are commonly used as ground-truth data for severe weather climatological studies, they are not perfect and are subject to bias (Doswell and Burgess 1988; Verbout et al. 2006). Additionally, Edwards et al. (2021) discussed issues involving changes in reported tornado path characteristics when the reporting system changed from using the F scale to the EF scale. These issues are somewhat less of a concern for significant, long-track tornadoes over this study period due to their greater socioeconomic impact, resulting in better documentation [e.g., National Weather Service (NWS) storm survey]. Nevertheless, every tornado case with a PL ≥ 30 mi was manually examined for accuracy using databases at NCEI, Storm Prediction Center (SPC), local NWS offices, and Grazulis (2023).

TABLE 1. Definitions for tornado PL in this study and traditional E(F) scale, along with number for each and number removed from filtering.

Category	Acronym	PL range	Number before filter (number after filter)	Number removed (percent removed)
Short track	STT	$0.01 \le$ PL $<$ 30 mi	47 738 (45 120)	2618 (5.5%)
Long track (generic)	LTT	PL $\ge$ 30 mi	474 (456)	18 (3.8%)
Long track	LTT	$30 \le$ PL $<$ 60 mi	399 (385)	14 (3.5%)
Very long track	VLTT	$60 \le$ PL$<$ 90 mi	61 (57)	4 (6.6%)
Extremely long track	XLTT	PL $\ge$ 90 mi	14 (14)	0 (0%)
Weak	E(F)0	PL $\ge$ 0.01 mi	26 457 (24 670)	1787 (6.8%)
Weak	E(F)1	PL $\ge$ 0.01 mi	15 561 (14 855)	706 (4.5%)
Significant	E(F)2	PL $\ge$ 0.01 mi	4644 (4524)	120 (2.6%)
Significant	E(F)3	PL $\ge$ 0.01 mi	1257 (1236)	21 (1.7%)
Violent	E(F)4	PL $\ge$ 0.01 mi	271 (269)	2 (0.7%)
Violent	E(F)5	PL $\ge$ 0.01 mi	22 (22)	0 (0%)
$0.01 \le$ PL $<$ 3 mi		$0.01 \le$ PL $<$ 3 mi	(31 573)	
$0.01 \le$ PL $<$ 10 mi		$0.01 \le$ PL $<$ 10 mi	(41 801)	
$10 \le$ PL $<$ 20 mi		$10 \le$ PL $<$ 20 mi	(2645)	
$20 \le$ PL $<$ 30 mi		$20 \le$ PL $<$ 30 mi	(674)	
$30 \le$ PL $<$ 40 mi		$30 \le$ PL $<$ 40 mi	(240)	
$40 \le$ PL $<$ 50 mi		$40 \le$ PL $<$ 50 mi	(101)	
$50 \le$ PL $<$ 60 mi		$50 \le$ PL $<$ 60 mi	(44)	
$60 \le$ PL $<$ 70 mi		$60 \le$ PL $<$ 70 mi	(29)	
$70 \le$ PL $<$ 80 mi		$70 \le$ PL $<$ 80 mi	(20)	
$80 \le$ PL $<$ 90 mi		$80 \le$ PL $<$ 90 mi	(8)	
$90 \le$ PL $<$ 120 mi		$90 \le$ PL $<$ 120 mi	(3)	
$120 \le$ PL $<$ 180 mi		$120 \le$ PL $<$180 mi	(11)	

After removing two highly unlikely longer-track cases (appendix A; there are potentially several more cases with erroneous PLs that have yet to be confirmed by NOAA), and cases where PL = 0 mi, E(F) scale = −9, and considering the contiguous United States (plus one 2019, 0.51-mi tornado in the Virgin Islands), a total of 48 212 tornadoes were used for the study. The tornado cases were stratified for further analysis into categories for PL as well as traditional E(F) scale, and these are defined in Table 1. Specifically, categories of long-track tornadoes are defined based on continuous PLs: $30 \le$ PL $<$ 60 mi ($48 \le$ PL $<$ 97 km), $60 \le$ PL $<$ 90 mi ($97 \le$ PL $<$ 145 km), and PL $\ge$ 90 mi ($\ge$145 km), respectively, and are also denoted collectively as long-track tornadoes, using guidance from SK22. Maps of the temporal and spatial frequencies of LTTs in the states and various geographical regions in the United States are provided in SK22.

b. *Reanalysis data*

Using each tornado report start time, 200+ variables were calculated from ERA5 reanalysis vertical profiles using the closest model grid point in space and time to the event by implementing the closest hour using a floor method described in Gensini et al. (2021). Note that the ERA5 reanalysis data have a horizontal resolution of ~31 km. The most representative vertical profile might be better represented at a midpoint time and a midpoint location; however, this was not done as only a start time and start location were consistently available for each tornado provided in either the SPC database (NCEI databases examined as a check) back to 1979. The ERA5 reanalysis dataset was chosen due to its superior vertical resolution of 137 hybrid-sigma levels (Hersbach et al. 2020). This allows for better representation of rapidly (time scales of 1 h) changing vertical profiles (e.g., sharp temperature inversions) that are vital to any vertically integrated calculations (e.g., CAPE and CIN). King and Kennedy (2019) showed ERA5 is as good or better than other reanalyses for analyzing convective variables with demonstrated mean correlations to observed soundings of 0.8 for thermodynamic parameters and 0.9 for kinematic parameters, respectively, while Taszarek et al. (2020a) showed ERA5 vertical profile data generally agreed well with observed data from rawinsondes.

The data were filtered for possibly contaminated or inaccurate profiles (boundaries, model forecast errors, temporal and spatial resolution, etc.) by removing those profiles with surface temperature < 8.0°C, most unstable CAPE (CAPEmu) $<$ 50 J kg^{-1} [from the surface through 500 mb (1 mb = 1 hPa)], and 10–6000-m bulk wind difference < 5 m s^{-1} (Brooks et al. 2007; Gensini et al. 2021). An additional filter was added to remove ERA5 vertical profiles when the reported SPC PLs and Bunkers' storm motions, used as a proxy for tornado forward speeds, resulted in tornado durations that were not consistent with known (or realistic) forward storm speed and duration extremes. This crude estimate of tornado path duration (PD) in minutes, based on Bunkers' internal dynamics (ID) storm speed V_{Bunkers} (Bunkers et al. 2000) and reported pathlength, is given by $\text{PD}_{\text{Bunkers}} = C_u \times \text{PL}/V_{\text{Bunkers}}$ (C_u is unit conversion factor C_u = 60.0/2.236 94 = 26.822 355, where 1 h = 60 min and 1 mph = 2.236 94 m s^{-1}). The filter is activated when $\text{PD}_{\text{Bunkers}} \ge \text{PD}_{\text{torn,max}}$, where $\text{PD}_{\text{torn,max}}$ = [70 + 1.1 × PL (mi)] (ad hoc PD threshold based on known

forward storm speed and duration extremes). Importantly, cases were not removed based on reported PLs, per se; rather, they were removed when the ERA5 vertical profiles resulted in PDs that were not representative or physically consistent with PDs and PLs for reasonably well-known observed extremes for durations found, for example, in Storm Data. The cases that were removed were likely associated with ERA5 forecast errors in physics, timing, and spatial evolution. Reported tornado durations were not in the SPC database, nor were they available for most cases in Storm Data, especially for earlier years (before the mid-2000s). Overall, for 10-mi bin increments from $0.01 \leq \text{PL} < 10$ mi to $70 \leq \text{PL} <$ 80 mi, 16, 10, 9, 3, 1, 3, 2, and 2 tornadoes were removed by this filter. The total of 46 tornadoes removed with this filter was ~0.0975% of all tornadoes in the SPC databases for 1979–2022, including 35 for PL < 30 mi, 11 for PL ≥ 30, and none for PL ≥ 80 mi. One of the cases removed had $\text{PD}_{\text{Bunkers}} >$ 912 min, another had $\text{PD}_{\text{Bunkers}} > 642$ min, 13 had $\text{PD}_{\text{Bunkers}} \geq$ 180 min [there are only two reports of tornadoes in the dataset with reported PDs longer than 180 min, both of which (Grazulis 2023; T. P. Grazulis 2021, personal communication) have been documented in ways that at least reasonably raised doubts whether the PLs were continuous; 134 mi F4 lasting a bit over 3 h on 7 June 1984 in Missouri and Iowa, and 160 mi F3 lasting for 3 h 15 min on 23 November 1992 in North Carolina; however we left these in the dataset], and 20 had $120 \leq \text{PD}_{\text{Bunkers}} <$ 180 min all with PL ≤ 80 mi. Importantly, this particular filter is not so aggressive as to remove some extreme cases such as the 28 May 2013 EF3 Bennington, Kansas Tornado [see "28 May 2013 Ottawa County Tornado," National Weather Service Office in Topeka, Kansas; National Oceanic and Atmospheric Administration (NOAA)-NWS 2013] that lasted for ~1 h and tracked 2.33 mi (3.75 km). All filters together resulted in 2636 cases (~5.5%) being removed, leaving a total of 45 576 vertical profiles. Sets of vertical profiles were also considered where a vertical profile was removed if the associated PL was <30 mi and the vertical profile was within ±1° latitude and longitude of longer-track tornadoes with a PL ≥ 30 mi, with and without the previously discussed filter; however, none of these other filtered sets resulted in meaningful changes to the results, even when these filters were either more limiting or more permissive (including just using unfiltered datasets).

c. *Analysis classification and variable definitions*

Numerous thermodynamic variables, including traditional thermodynamic-based parameters, traditional kinematic-based tornado proximity sounding parameters, and composite thermodynamic-wind parameters, were examined in this study (Table 2). These parameters are commonly used in both tornado research and operational tornado forecasting.

Thermodynamic (lowest 1000 m AGL used to define the mixed layer), kinematic, and composite parameters were evaluated using box-and-whisker plots [whiskers are at Q1 − 1.5 IQR and Q3 + 1.5 IQR; box edges are the Q1 = 25th and Q3 = 75th percentiles, Q2 = median, and IQR is the interquartile range] to demonstrate associations with respect to tornado PLs in length bins (i.e., 0.01–3, 0.01–10, 10–20, … , 80–90, ≥90, 30–60, 60–90, 90–120, and 120–180 mi). Bins for the E(F) scale [E(F)0, E(F)1, E(F)2, E(F)3, E(F)4, and E(F)5] were also generated for comparison with previous studies of tornadic storms, as well as for evaluation in the context of long-track tornadoes. The E(F)-scale comparisons were relevant as longer-track tornadoes tended to be stronger tornadoes (SK22). Additionally, longer-track tornadoes tended to produce more death and injuries and achieved higher damage ratings owing to a greater chance to reveal intensity and produce death and injuries (SK22). As noted by C19, various popular sounding analysis software packages give CAPE values that can vary by as much as 200–500 J kg^{-1}, while calculations for kinematic parameters are comparable (C19 noted CAPE values were largest with the NSHARP/SHARPpy packages developed by Hart and Korotky 1991; Blumberg et al. 2017). Given the issues discussed by C19 regarding CAPE, which have been found by the authors here to be related at least in part to the equations used for approximating CAPE, latent heat values (temperature dependent), and to a lesser degree by the gravitational acceleration value as well as definitions for specific heats and other gas constants, herein CAPE, CIN, LCL, LFC, etc. (thermodynamic parameters), were calculated from the ERA5 vertical profiles by lifting parcels with an increment of $\delta p = 50$ Pa (0.5 mb; or roughly 4–6 m depending on distance from the ground) in George Bryan's "getcape.f90" FORTRAN 90 source code, which integrates the thermodynamic equation (e.g., Bryan and Fritsch 2004; Cotton et al. 2010). We considered only liquid processes, noting that including ice processes could increase CAPE values by upward of roughly 3%–8% or more (Cotton et al. 2010). Bryan's code was also modified to calculate downdraft cape (DCAPE, not used here) and mixed-layer 0–3000-m CAPE (CAPE03ml). All vertically integrated storm-relative and related wind values were computed after linearly interpolating ERA5 winds to a vertical grid with 5-m resolution and subtracting the Bunkers' et al. (2000) ID storm motion. Results for effective inflow layer quantities were not considered for tornadic supercells, although the effective inflow layer concept was developed as a way to estimate ESRH in the deep inflow layer of tornadic supercells, as well as to approximate inflow layers in environments that support elevated supercells with inflow from above the surface (T07). For a comprehensive comparison of thermodynamic and wind-related sounding parameters between tornadic and severe wind/hail-producing storms, readers are directed to T20b.

d. *Statistical guidance*

Statistical guidance (additional technical details are provided in the online supplemental material) in this study employed:

1) The Student's *t*-test statistics for the difference in mean *p* values (significance here defined as $p \leq 0.001$; linearly interpolated from published tabulated values; *p*-value results and means are provided in appendix B) are used and most relevant for normal distributions. Consideration of whether variances are comparable (ratios less than 2) or not (ratios greater than 2) is used to compute *t*-test statistics [when ratios are greater than 2, the Welch's *t* test (Welch 1947) generalization of the Student's *t* test is used;

TABLE 2. Severe weather parameters evaluated from ERA5 vertical profiles, with units and references (nondim = nondimensional).

	Parameter	Units	Reference examples
CAPEml	Convective available potential energy in lowest 1000 m, approximating the mixed layer (ml)	J kg^{-1}	Doswell and Rasmussen (1994); Cotton et al. (2010)
CAPE03ml	0–3-km CAPEml	J kg^{-1}	Rasmussen (2003)
CAPEmu	Most unstable (mu) CAPE	J kg^{-1}	Evans and Doswell (2001)
CINml	Convective inhibition (mixed layer)	J kg^{-1}	Davies (2004)
LCLml	Lifting condensation level in lowest 1000 m (mixed layer)	m	Doswell and Rasmussen (1994); Cotton et al. (2010)
WSSFC, WS500, …, WS10000, WSLLmax, WSULmax	Wind speed [surface (10 m), 500, 1000, 2000, …, 10 000 m, low-level max 200–2000 m, upper-level max 5000–9000 m]	m s^{-1}	Markowski et al. (2003)
BWD500, …, BWD10000, BWDLLmax, BWDULmax	Bulk wind difference or vector shear (10–500, 10–1000, 10–200, …, 10–10 000 m, max between 10 and 200–2000 m, max between 10 and 5000–9000 m)	m s^{-1}	Rasmussen and Blanchard (1998); T03; T07; Davies and Johns (1993)
SRH500, SRH1000, …, SRH6000	Storm-relative helicity (10–500, 10–1000, 10–2000, 10–3000, 10–4000, 10–6000 m)	m^2 s^{-2}	Davies-Jones et al. (1990); C19; Davies and Johns (1993)
SRWSSFC, SRWS500, …, SRWS10000	Storm-relative winds speeds (same levels as wind speeds)	m s^{-1}	Davies-Jones et al. (1990); Thompson (1998); Brooks et al. (1994)
SRMLIKE	Storm-relative mean-layer inflow kinetic energy	m^2 s^{-2}	Herein
V_{Bunkers}	Bunkers' ID storm motion (direction; speed)	°; m s^{-1}	Bunkers et al. (2000)
Bunkers' time	Bunkers' ID tornado duration [C_{unit} = PL (mi)/V_{Bunkers} = 60.0/2.236 94 = 26.822 355 5]	min	Based on observed PL and V_{Bunkers}
EHI500	Energy–helicity index (10–500-m SRH)	nondim	Hart and Korotky (1991)
STPcin500, STPcin1000	Significant tornado parameter with CAPEml, CINml, and 10–500- and 10–1000 m-SRH	nondim	T07
VTPcin500, VTPcin1000	Violent tornado parameter with CAPEml, CINml, and 0–500- and 10–1000 m-SRH	nondim	Hampshire et al. (2018)
CA500	Critical angle (10–500 m)	°	Esterheld and Giuliano (2008)

see appendix B]. Cohen's d values of 0.2–0.5, 0.5–0.8, and >0.8 are used for common language small, medium, and large effect sizes (Cohen 1988; the importance of differences in the means; d values and standard deviations for results are in appendix C) for the Student's t-test statistics. Absolute values of Pearson's skewness > 0.4 (supplemental material) provided an indication of nonnormal distributions.

2) Mann–Whitney U statistics (MWU; Mann and Whitney 1947; Kasuya 2001; Nachar 2008) [described as the "probability that a randomly sampled observation from the first group is less than a randomly sampled observation from the second group," Wilcox (2023)] p values (significant here defined as $p \leq 0.001$; results are provided in appendix D) are used to interpret nonnormal distributions (with or without logarithmic transformation). A common language effect size is provided by f values [f = U1/($n_1 \times n_2$), where U1 is the U value for the unique sample with shorter PLs; results are provided in appendix E]. The value 1) $f = 0.7$, as defined above, based on all pairwise matchups between two independent samples, means that 70% of the matchups of values in sample 1 are smaller than those in sample 2 (30% overlap); 2) $f = 1$ means all, or 100%, of the matchups of values in sample 1 are smaller than in sample 2 (no overlap in distributions); 3) $f = 0.5$ means no better than random chance (complete overlap of the two distributions); and 4) $f = 0.0$ means all matchups of values in sample 1 are larger than those in sample 2 with no overlap of the samples, which is worse than chance (or perfect if the definition is reversed, which means 100% of the matchups of values in sample 1 are larger than in sample 2). Note that f values are equivalent to area under the curve (AUC) statistics for MWU, as are their respective interpretations. The rank-biserial correlation [r = 2U1/($n_1 \times n_2$) − 1 = 1 − 2U2/($n_1 \times n_2$);

results are in appendix F] used to indicate the "correlation between the fraction of favorable pairs minus the fraction of unfavorable pairs from two independent samples" was also provided. Small, medium, and large are common language effect sizes when r values = 0.1–0.3, 0.3–0.5, and >0.5 (negative r values indicate an inverse relation), keeping in mind that r values range from −1 to 1 and that the r values for effect size can be problem dependent.

3) The maximum true skill scores (TSS_{max}) along with the associated optimum values (Opt. at TSS_{max}) of parameters are also provided (appendix G) and often used in the type of study presented in this paper. The definition of TSS is given as $TSS = [(YY)(NN) - (NY)(YN)]/[(YY + NY) \times (NN + YN)]$, where the first letter in each letter pair indicates the forecast and the second indicates the truth, with Y = yes (true or correct) and N = no (false or incorrect), respectively, YY is the sum of the number of correct forecasts of an event, YN is the sum of the number of forecasts of an event that did not occur (false alarm), NY is the sum of the number of missed (incorrect) forecasts of an event, and NN is the sum of the number of correct forecasts of no events occurring (correct null forecasts). C19 state, "The TSS highlights parameters that maximize probability of detection (POD; or 'hit rate') while minimizing probability of false detection (POFD [probability of false detection]; or 'false alarm rate')." This idea was also discussed in Doswell et al. (1990) and others. Values herein of TSS_{max} = 0.2–0.6, 0.6–0.8, and >0.8 can be interpreted as low, medium, and high forecast skills (Allouche et al. 2006; Komac et al. 2016). The TSS_{max} values, or optimum values, were determined from TSS values from 1000 values of a parameter from equally spaced intervals from roughly Q1 − 1.5 IQR to Q3 + 1.5 IQR of any 10-mi PL subcategory or E(F)-scale category in the data.

The statistical power (the power to detect meaningful differences between two populations) of the statistics used can be approximated herein by their effect sizes. In this manner, larger effect sizes indicate larger differences from the statistical hypotheses and vice versa. When effect sizes are small, larger populations are needed to potentially indicate differences; otherwise, the differences are not meaningful. The statistical quantities discussed above are provided with cautions that their limitations must be fully considered for reasonable inferences. While none of these statistics were seemingly superior compared to another in this study in a relative sense, the MWU statistics were the most optimistic and the values of TSS_{max} were the least optimistic.

4. Results

a. Thermodynamic sounding parameters

Box-and-whisker plots and scatter diagrams of mixed-layer CAPE (CAPEml), CAPEmu, CAPE03ml, mixed-layer CIN (CINml), and mixed-layer LCL (LCLml) were used to provide guidance for comparing sounding parameter values versus PLs, and E(F) for the former [Fig. 1; hereafter, Q1, Q2 (median), and Q3 represent the 25th, 50th, and 75th percentiles, respectively]. The scatter diagrams include linear fits for PL ≥ 0.01, PL ≥ 30, and PL < 30 mi and the associated values of the square of Pearson's correlation denoted as R_2 or common variance. Quadratic, cubic, exponential, power, and other fits were tried and these generally produced lower R_2 values than linear fits.

Median values of CAPEml tended to increase with longer PLs and especially with larger E(F)-scale ratings in a range typically from 500 to 1500 J kg^{-1} and only rarely to values > 2700 J kg^{-1}. Larger separations of median CAPEml with increasing PL did not occur until PLs exceeded 50 mi. Previous studies have shown that stronger tornadoes are often associated with larger values of CAPEml (T03), but not always. As shown by SK22, tornadoes with PL ≥ 30 mi more typically produced ≥E(F)3 damage and PL ≥ 60 mi more typically produced ≥E(F)4 damage; hence, unsurprisingly, somewhat larger CAPEml values were associated with longer-track tornado PLs. While there was substantial overlap in CAPEml values for all tornado PLs and much spread in CAPEml values below the medians for longer-track tornadoes (some of which were likely associated with poor representation of the true atmosphere near surface boundaries in the ERA5 analyses), there was a cluster of rather modest CAPEml values around 500–1200 J kg^{-1} for PL ≥ 30 mi (mostly in the southeast United States). Some of the CAPE signals might be associated with a possible low damage-rating bias for Great Plains tornadoes (e.g., few structures damaged even though mobile radar winds suggest higher wind speeds than the damage rating; Wurman et al. 2021).

An association with increasing tornado PLs was also seen for increasing (decreasing) values of CAPEmu and CAPE03mu (LCLmu) (Fig. 1; the latter two not shown), and these all were comparable, especially CAPEmu, when PL was compared to CAPEml, CAPE03ml, and LCLml, across the PL stratifications. Pathlength stratifications showed CAPE03ml increased when comparing PL < 10 mi to longer PL stratifications, especially for 30 ≤ PL < 60 mi and 60 ≤ PL < 90 mi. There were also somewhat lower values of LCLml (as well as 0–500-m mean relative humidity, not shown, provided in the supplemental material) for longer-track tornadoes than for shorter-track tornadoes. Expectedly, significant tornadoes rated E(F)2–5 were generally associated with lower LCLml heights as found in previous studies. Finally, note the smaller relative differences with CINml between shorter-track and longer-track tornadoes than with CAPEml, with somewhat smaller values of CINml for tornadoes with PL ≥ 60 mi (many of these occurring in the southeast United States during the cool season, geographical coverage not shown).

The box-and-whisker plots show that CAPEml values at Q3 (Q3 + 1.5 IQR) were ≤1613 J kg^{-1} (3120 J kg^{-1}) in the ERA5 vertical profiles using the PL bins, while outlier-extreme events (outside whiskers) occurred with values of CAPEml ≥ 3120 J kg^{-1}. Additionally, CAPE03ml, CINml, and LCLml values for most tornadoes based on PL bins at Q3 (Q3 + 1.5 IQR) values were ≤100 (185) J kg^{-1}, ≤ 65 J kg^{-1} (145 J kg^{-1}), and ≤ 1200 m (2100 m), respectively. Using the E(F)-scale bins, CAPEml, CAPE03ml, CINml, and LCLml values at Q3 (Q3 + 1.5 IQR) values were ≤2650 J kg^{-1} (3550 J kg^{-1}), ≤105 J kg^{-1} (185 J kg^{-1}), ≤65 J kg^{-1} (145 J kg^{-1}), and ≤1250 m (2200 m), respectively. Some of the longest

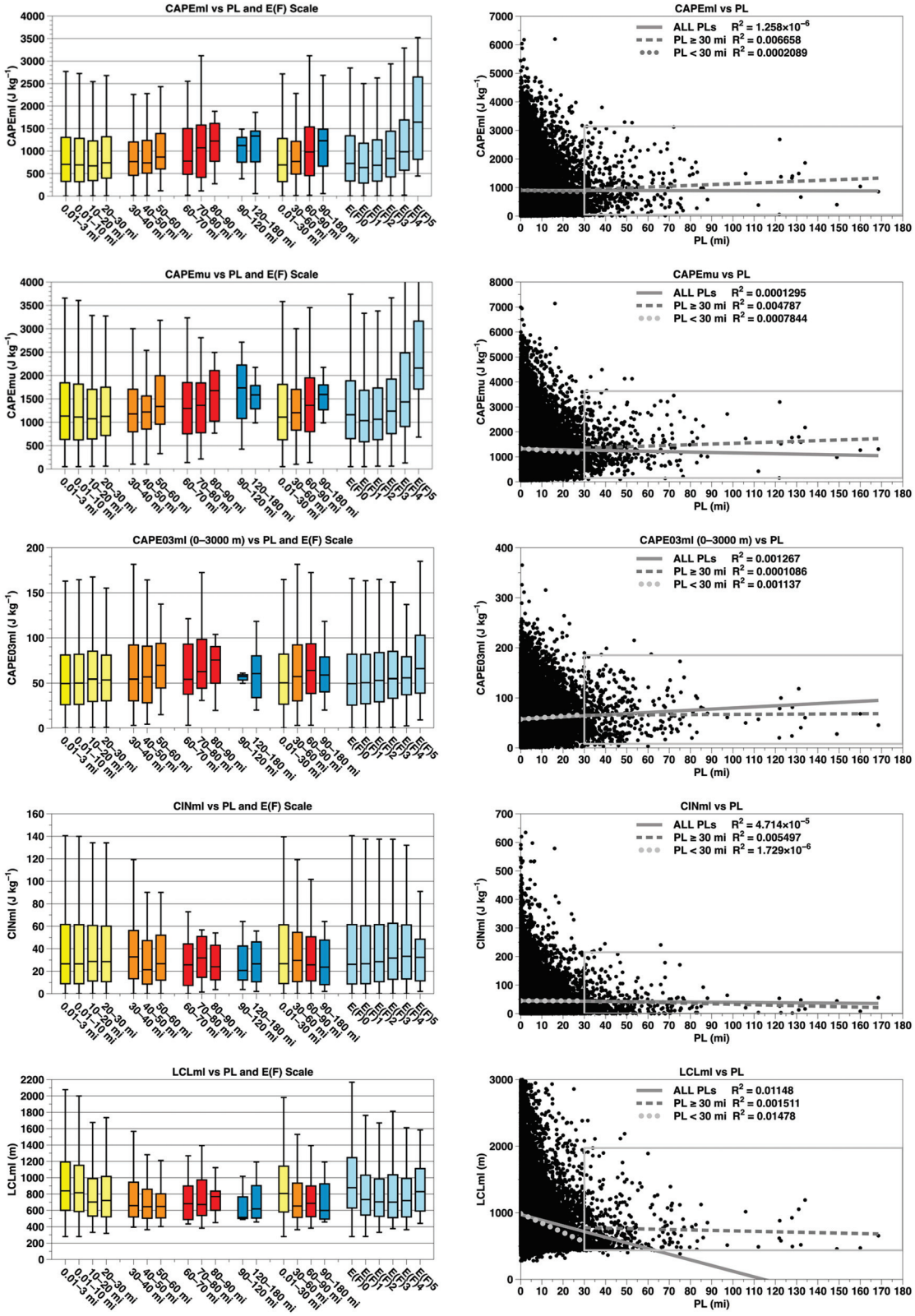

FIG. 1. Box-and-whisker plots and scatter diagrams with linear-fit and R^2 values for all PLs (solid line and top R^2), PL ≥ 30 mi (dashed line and second R^2), and PL < 30 mi (dotted line and third R^2), as well as a long rectangle around values for PL ≥ 30 mi (five largest and five smallest values are excluded; ~97.5% of the PL ≥ 30 mi cases are represented inside the rectangle) of CAPEml (J kg^{-1}), CAPEmu (J kg^{-1}), CAPE03ml (J kg^{-1}), CINml (J kg^{-1}), and LCLml (m). The whiskers are at Q1 − 1.5 IQR and Q3 + 1.5 IQR, the box edges are the 25th and 75th percentiles, and the horizontal lines in the boxes are the median values. Outliers are not shown. Numbers in each 10-mi bin are in both Table 1 and supplemental Table 8.

individual tornado PLs were associated with environments that had values in or above the upper quartile range for CAPE03ml and CINml and the lower quartile range for LCLml. Nevertheless, the mixed-layer thermodynamic parameter results associated with longer-track tornadoes were generally consistent with G07 and G21 and with B06 for longer-lived supercells.

Overall, box-and-whisker plots for thermodynamic variables depicted a more robust separation between PL categories compared to scatterplots, which showed substantial scatter and no separation between PL values (Fig. 1; right column). The linear-fit R^2 was effectively zero for CAPEml, CINml, CAPEmu, CAPE03ml, and LCLml (the latter two not shown) and only slightly better for CAPE03ml and LCLml. Almost all thermodynamic variables were expectedly skewed (>0.40) with long tails to the right. Therefore, the use of the Student's *t*-test-associated *p* values and Cohen's *d* values might not be appropriate. Keeping this in mind, CAPEml for various PL comparisons have Student's *t*-test p values ≤ 0.05 only when comparing PL $<$ 10 mi to PL $\geq$ 30 mi, and PL $<$ 30 mi compared to PL $\geq$ 30 mi, while Student's *t*-test *p* values were higher for CAPEmu. The Student's *t*-test *p* values were somewhat better for CAPE03ml with p values < 0.001 when comparing PL $<$ 10 mi to PL $\geq$ 10, PL $\geq$ 30, and 30 $\leq$ PL $<$ 60 and 30 $\leq$ PL $<$ 90 mi, as well as PL $<$ 30 mi compared to PL $\geq$ 30. Additionally, there was $p \leq 0.001$ for LCLml among most of the PL comparisons. The very small-to-medium–small effect size (0.49 for LCLml and 0.57 for LFCml) for all thermodynamic variables based on *d* values suggests the smallest of these, some of which were associated with p values < 0.05, were not very important based on differences in mean values. Additionally, the small p values ≤ 0.001 for LCLml and LFCml (LFCml in supplement) also were associated with lower *d* values that suggested only small-to-medium–small importance. For comparison with the Student's *t*-test statistics, the MWU *p* values for both CAPEml and CAPEmu were mostly ≤ 0.05 (some were ≤ 0.001), with f values = 0.501–0.634 and r values = 0.002–0.267, and thus had only small effect size; thus, CAPEml and CAPEmu were generally not statistically important for indicating PL. Also, the Student's *t*-test and MWU *p* values were similar for CAPE03ml, LCLml, LFCml, and CINml except when comparing the latter for PL $<$ 10 mi to PL $\geq$ 10, where MWU *p* values indicated some significance at 0.001 with mostly small effect size based on MWU f and r values. There were some f values < 0.5 as well as r values < 0, indicating an inverse relation between LCLml, LFCml, and CINml, especially for the former two, and PL. These statistical results are consistent with all $\text{TSS}_{\text{max}} \leq 0.306$ for CAPEml, $\leq$0.351 for CAPEmu, and absolute values for $\text{TSS}_{\text{max}} \leq 0.307$ for LCLml, LFCml, and CINml.

The substantial overlap in box-and-whisker plots and scatter diagrams and small effect size statistical measures suggests that large CAPEml and low CINml are of lesser importance when discriminating between especially LTT environments and perhaps tornadoes in general or between tornadic and nontornadic environments (Rasmussen and Blanchard 1998; C19; T20a), although there is notable signal for E(F)3+ tornadoes (see also Hampshire et al. 2018; C19; T20a). Nevertheless, one might wonder whether CAPE is more of a proxy for the potential for deep convection (see also C19; Hill et al. 2020), and nothing more, and perhaps not physically related, except maybe in a weak way, to potential tornado strength in some cases. Perhaps synoptic or mesoscale environments with larger shears, which support stronger tornadoes and/or longer-track tornadoes, were climatologically more likely to have larger values of CAPE. It is worth adding also that C19 found that CAPE itself was not very skillful at differentiating between nontornadic and significantly tornadic supercells; many tornadoes are associated with a high-shear low-CAPE regime (e.g., Sherburn and Parker 2014), and one of the main benefits of CAPE is that it delineates between where deep convection is possible and where it is not (Hill et al. 2020).

In summary, thermodynamic parameters used here such as CINml, LCLml, and LFCml were not useful to indicate tornado pathlength in general; however, CAPEml or CAPEmu could be useful once PL exceeded 70 mi; however, the effect sizes for the Student's *t*-test or MWU statistics were at best medium in these instances. Finally, TSS_{max} values indicated the same relative degree of importance as other statistics for thermodynamic parameters.

b. *Kinematic sounding parameters*

Longer-track tornadoes were ubiquitously associated with larger tropospheric wind speeds, although environments with higher wind speeds did not always translate to longer-track tornadoes given that many shorter-track tornadoes were often associated with higher wind speeds. Median wind speeds at 500, 1000, 4000, 6000, and 9000 m, overall, however, were found to be up to 41% larger for longer-track (30 $\leq$ PL $<$ 60 mi) tornadoes than shorter-track (0.01 $\leq$ PL $<$ 30 mi) tornadoes (Fig. 2), with somewhat larger increases of up to 47% found for wind speeds in the lower ($z \leq 2000$ m), mid ($2000 < z \leq 5000$ m), and upper ($z > 5000$ m) levels for very-long-track tornadoes (60 $\leq$ PL $<$ 90 mi) compared to shorter-track tornadoes (0.01 $\leq$ PL $<$ 30 mi). Importantly, no longer-track tornadoes (PL $\geq$ 30 mi, based on 10-mi bin increments) occurred with 500-, 1000-, 4000-, 6000-, and 9000-m ground-relative wind speeds at the 25th percentile that were below 13, 16, 24, 27, and 30 m s^{-1}, respectively. Furthermore, no tornadoes with PL $\geq$ 60 mi (based on 10-mi bin increments) occurred with 500-, 1000-, 4000-, 6000-, and 9000-m wind speeds at the 25th percentile that were below 13, 18, 25, 29, and 32 m s^{-1}, respectively. Based on the 30-mi bin increments, the wind speeds overall (all heights) were ~6–10 m s^{-1} lower at the 25th percentile for PL $<$ 30 mi than for PL $\geq$ 30 mi, ~6–14 m s^{-1} lower at the 25th percentile for PL $<$ 30 mi than for 60 $\leq$ PL $<$ 90 mi, and ~12–15 m s^{-1} lower at the 25th percentile for PL $<$ 30 mi than for PL $\geq$ 90 mi. These results were supported by the scatter diagrams for above-surface wind speeds versus PLs and both the Student's *t*-test and MWU *p* values mostly $\leq$0.001, which were further supported by medium-to-large effect size based on *d* values mostly $\geq$0.5 with many *d* values $\geq$ 0.8 for the Student's *t*-test statistics, while f values ranged from 0.599 to 0.921 and r values ranged from 0.197 to 0.841 for MWU. Expectedly, the largest f values and r values were associated with comparisons between PL $<$ 10 mi and PL $\geq$ 90 mi, followed by PL $<$ 10 mi

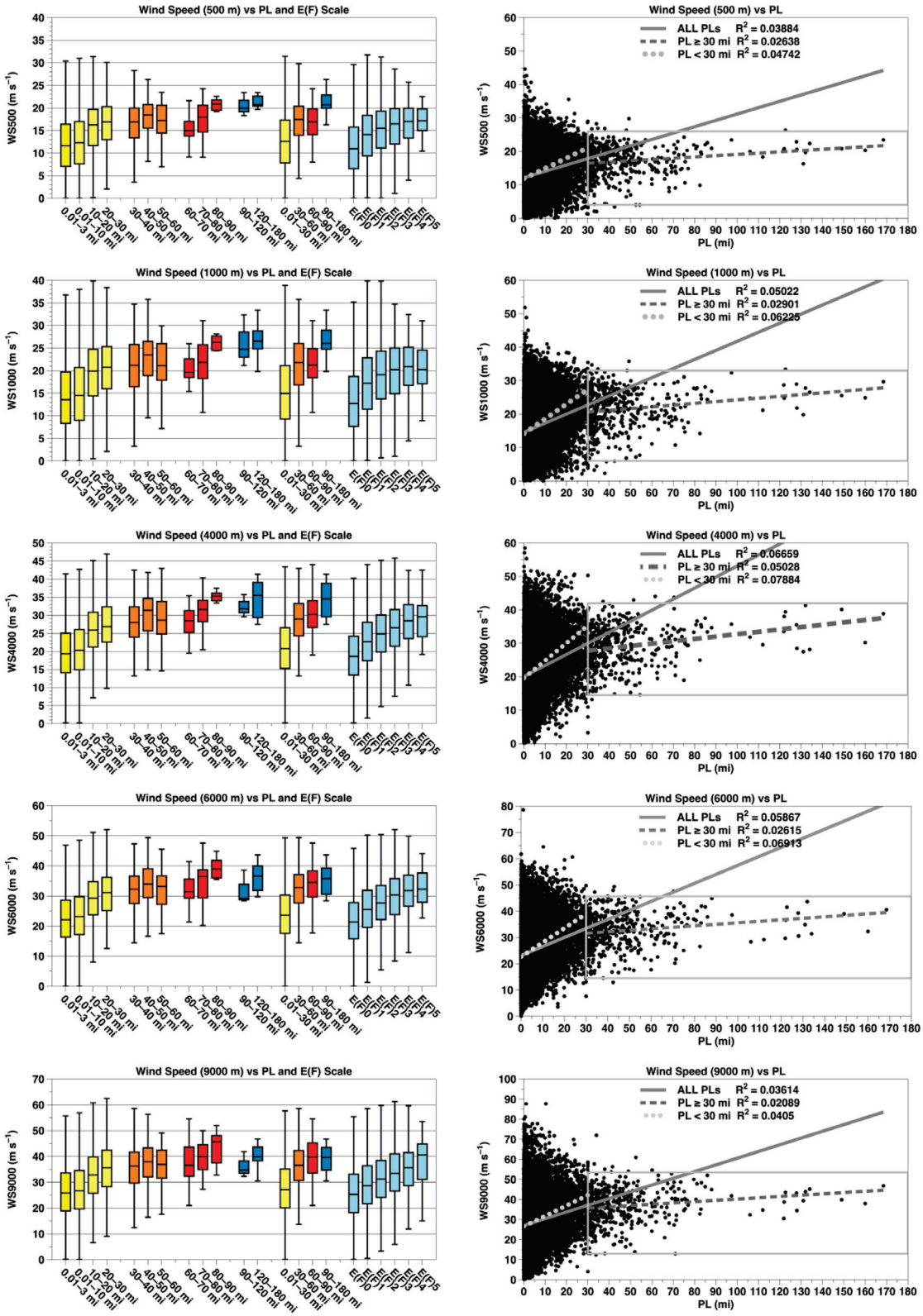

FIG. 2. As in Fig. 1, but for ground-relative wind speed (m s^{-1}) at 500, 1000, 4000, 6000, and 9000 m.

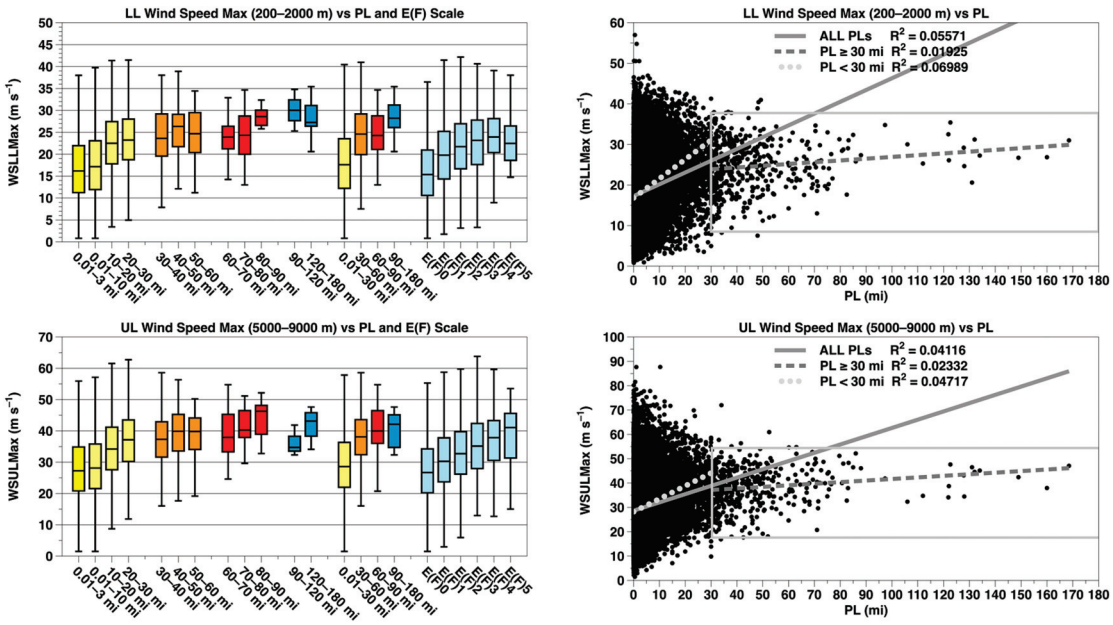

FIG. 3. As in Fig. 1, but for maximum wind speed (m s^{-1}) between 200 and 2000 m, which represents the low-level wind speed maximum (or an appropriate low-level jet maximum), and maximum wind speed between 5000 and 9000 m, which approximates an upper-level wind speed maximum.

and $60 \leq PL < 90$ mi. With the majority of r values ≥ 0.3 and many ≥ 0.5, the common language effect size was generally medium to large. The trends for TSS_{max} were consistent with the other statistics and, to a lesser extent, with MWU. Finally, the statistics employed show there were generally favorable advantages, albeit slightly, to defining LTT supportive lower-, mid-, and upper-level wind speeds with the 200–2000-m maximum, 4000, and 5000–9000-m maximum, than using wind speeds at other levels.

Unlike thermodynamic variables, with distributions that were largely skewed to the right, the wind speed distributions were more normal like in shape as indicated by mostly smaller absolute skewness < 0.3 (see table in supplemental material). Small negative skewness values for the wind speed distributions indicated the distributions were more normal in shape, which were generally slightly skewed with a tail toward smaller values for most PL bins, except for PL ≥ 90 mi, which had positively skewed distributions for wind speeds at the surface, 500, 1000, 2000, and 3000, while the PL $<$ 10-mi and PL $<$ 30-mi bins were positively skewed at most levels. Maximum wind speeds at lower and upper levels tended to be better represented by the maximum wind speed between 200–2000 m for the low levels and 5000–9000 m for the upper levels (Fig. 3). Longer-track tornadoes were also associated with larger mean wind speeds in all the various layer depths considered between 10 and 9000 m (Fig. 4). Additionally, wind speeds above 1 km showed an approximate monotonic increase for E(F)2+ tornadoes.

Importantly, the association between Bunkers' ID storm speed and Bunkers' duration (based on reported PL and calculated Bunkers' ID storm speed; Fig. 5) with PL was both significant for p values < 0.001 and supported by medium-to-large (and very large) d values (0.7–1.58) for the former, and very large d values (3.53–27.61) for the latter, for all PL bins compared. Additionally, MWU f values were ≥ 0.98 and r values were ≥ 0.96 for Bunkers' duration for all PL bins. Based on these statistics and the high correlation ($R^2 = 0.79$) for tornado PLs and Bunkers' ID storm durations (Fig. 5), if an approximate storm mesocyclone temporal periodicity could be predicted, even for an isolated storm, perhaps an approximate tornado PL could be better anticipated using Bunkers' ID storm speed. However, this result on its own would not be useful for forecasters, because it would require a priori knowledge of PL. Thus, these results were hindsight biased due to known PLs. Nevertheless, the strong relation between storm duration and PL provides motivation for efforts to better anticipate mesocyclone periodicity. Thus far, mesocyclone periodicity has proven to be notoriously difficult to understand, anticipate, and forecast (Adlerman et al. 1999; Britt et al. 2020).

Discrimination of PL categories was also partially possible using surface (10 m) storm-relative (SR) wind speeds, which were notably smaller amplitudes for shorter-track tornado PLs than for longer-track tornado PLs (Fig. 6). Faster-moving storms also generally were associated with larger storm-relative surface wind speeds (which is associated with faster storm motions), with $R^2 = 0.87$ between surface storm-relative wind speeds and Bunkers' ID storm motion (not shown). The 10–8000-m mean wind speed and the 4000-m wind speeds also had the highest R^2 values with Bunkers' ID storm motion (0.81 and 0.82, respectively, not shown), which are larger than the R^2 values between 10- and 6000-m mean wind speeds and Bunkers' ID storm motion (0.80). In contrast, storm-relative wind speeds at 6000 m (Fig. 6) were very weakly associated (uncorrelated, with $R^2 < 9.9 \times 10^{-4}$) with both tornado PL and E(F)-scale rating, suggesting they were not particularly well associated with these tornado attributes.

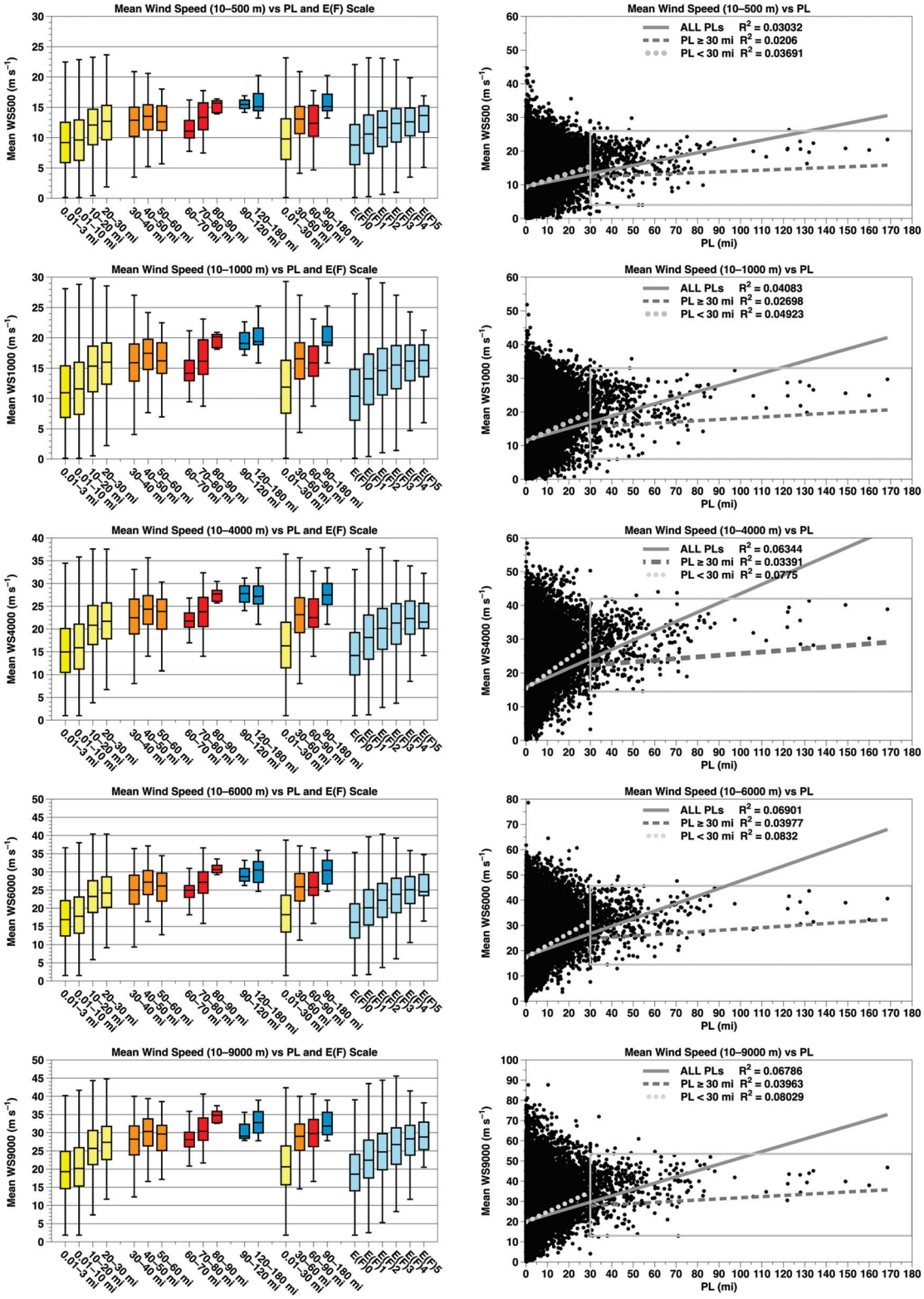

FIG. 4. As in Fig. 1, but for mean wind speed (m s^{-1}) between 10–500, 10–1000, 10–4000, 10–6000, and 10–9000 m.

Expectedly, weak associations in storm-relative wind speeds at 6000 m (and most levels above ~500 m and below 6000 m; statistics in supplemental material) result, in part, from using Bunkers' ID storm motion, which is dependent on the wind speeds between the surface and 6000 m and a 7.5 m s^{-1} orthogonal propagation vector (through the mean surface to 6000-m wind speeds with a component orthogonal to the surface to 6000-m shear vector). The R^2 values also were quite

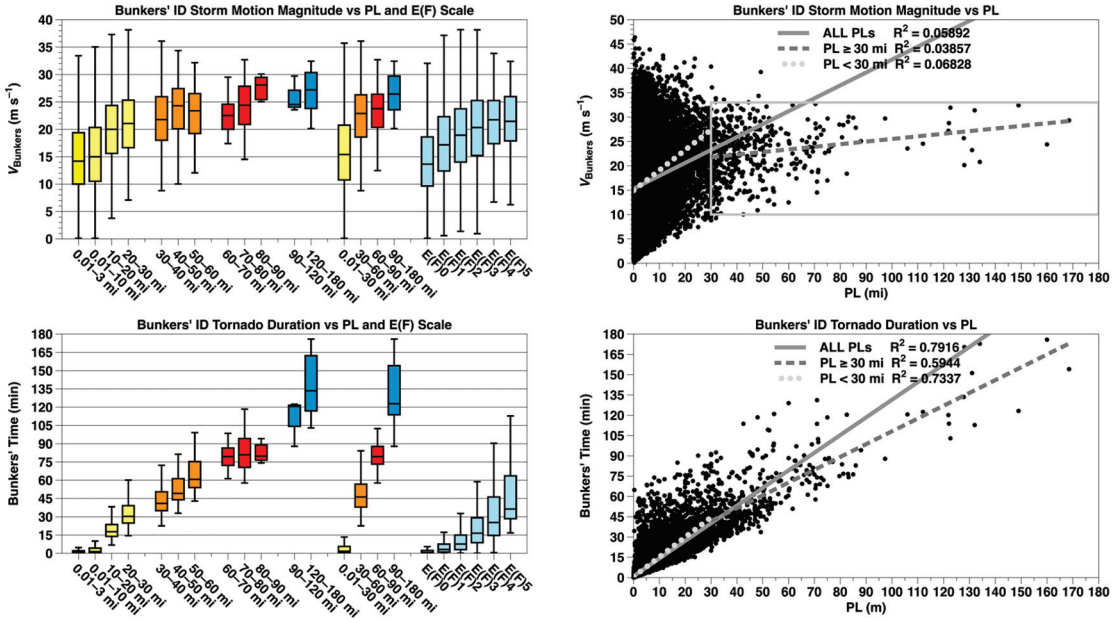

FIG. 5. As in Fig. 1, but for Bunker's ID storm speed (m s^{-1}) and Bunker's duration (min).

small $< 3 \times 10^{-4}$ (uncorrelated) between storm-relative flow above 6000 m (not shown) and both tornado PL and E(F)-scale rating. An upper-level wind profile with only minor increases in wind speeds above the midlevels was reminiscent of the upper-level wind profile associated with a small population of high-precipitation supercells (Rasmussen and Straka 1998). B06, however, reported that weaker shears aloft were associated with shorter-lived (<2 h) supercells (compare their Fig. 5), which was not necessarily inconsistent with weaker storm-relative flows aloft with longer-track tornadoes. Thus, while B06 suggested that weak storm-relative winds aloft may favor shorter-lived supercells, this finding did not exclude the possibility of longer-lived supercells with long-track tornadoes.

Similar to the wind speed results at various levels, longer tornado PLs and larger E(F)-scale ratings were often associated with larger BWDs (m s^{-1}) between 10–500, …, 10–9000 m (Fig. 7), as well as with the maximum BWD between 10 m and 200–2000 m for lower levels and the maximum BWD between 10 m and 5000–9000 m for upper levels (Fig. 8). These results for BWD are supported by the scatter diagrams and both the Student's *t*-test and MWU *p* values ≤ 0.001 and further supported by generally medium-to-large *d*, *f*, and *r* values, for

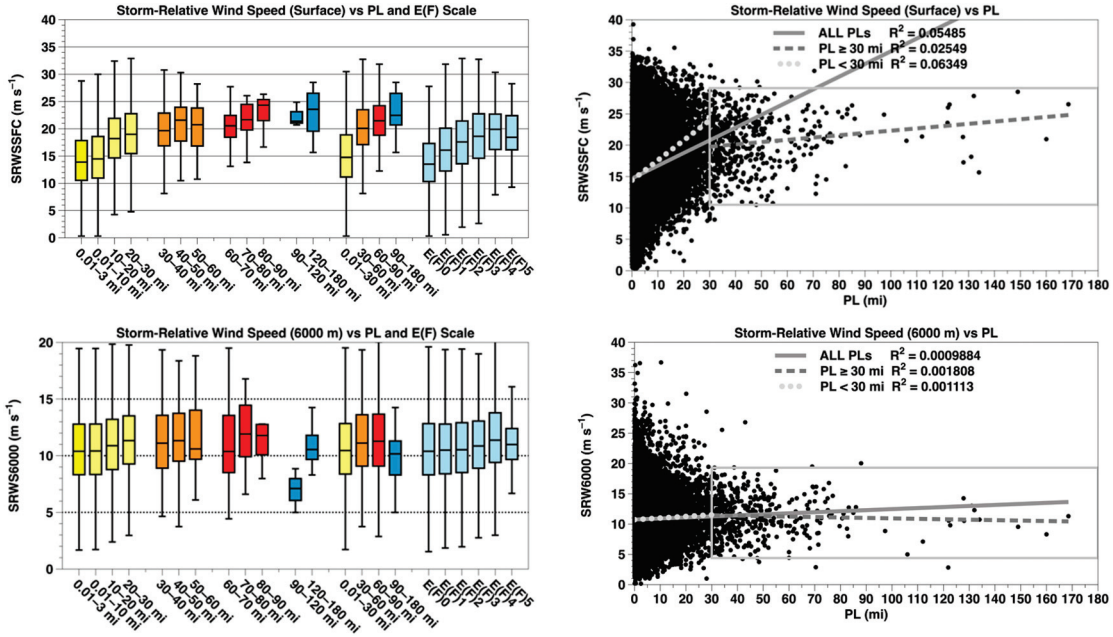

FIG. 6. As in Fig. 1, but for surface (10 m) and 6000-m storm-relative wind speed (m s^{-1}).

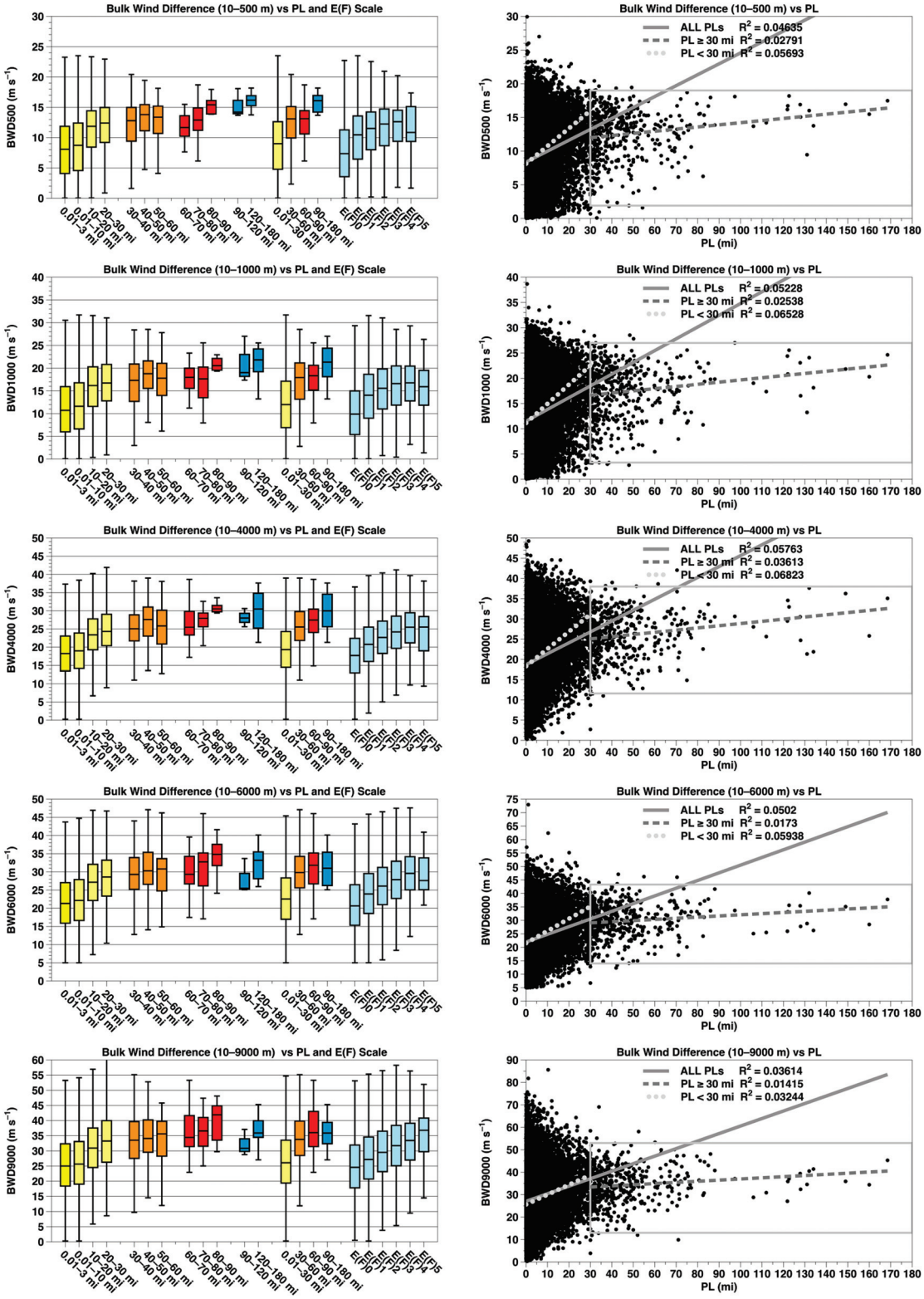

FIG. 7. As in Fig. 1, but for bulk wind speed difference (BWD; m s^{-1}) for 10–500, 10–1000, 10–4000, 10–6000, and 10–9000 m.

most comparisons between various PL bins. Importantly, as expected, the skewness of the BWD distributions approximately resembled those for wind speeds, except for the BWD values in the lowest layers for the longest pathlength bins, which have BWD distribution skewed more to the left, with BWD values clustered toward higher values, consistent with long-track tornadoes being more associated with stronger low-level BWD and wind speeds. The box-and-whisker plots showed slightly

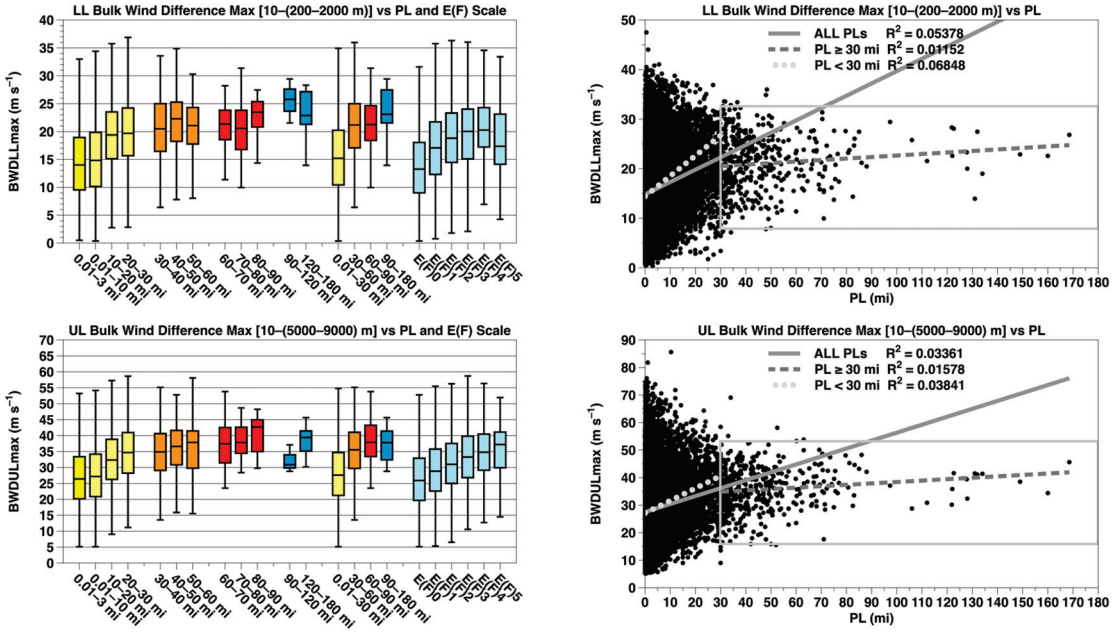

FIG. 8. As in Fig. 1, but for maximum bulk wind speed difference (m s^{-1}) between 10 and 200–2000 m and maximum BWD between 10 and 5000–9000 m.

better discrimination in some instances between PL categories with maximum BWD from lower and upper levels (Fig. 8) than BWD values at constant-height levels (Fig. 7). There is a very clear signal for threshold BWD shear values for longer-track tornadoes (PL ≥ 30 mi) as seen in both the box-and-whisker plots and the scatter diagrams (discussed more below). Like with wind speeds, all statistics employed show there were also general advantages, albeit slightly, to defining LTT supportive lower-, mid-, and upper-level BWDs with the 500, 4000, and 5000–9000-m maximum, than using other BWDs.

Larger values of SRH500, SRH1000, and SRH3000 were associated with longer-track tornadoes, as well as more significant tornado damage ratings (Fig. 9). While SRH discriminated well between tornadoes with 0.01 ≤ PL < 30 mi and 30 ≤ PL < 60 mi, there was only weak discrimination capability between various 10-mi tornado PL bins, except for 0.01 ≤ PL < 10 mi compared to 10 ≤ PL < 20 mi, and 70 ≤ PL < 80 mi compared to 80 ≤ PL < 90 mi. The stronger association of longer-track tornadoes with larger SRH values was perhaps consistent with longer-track tornadoes being more significant E(F)2+ or violent E(F)4+. Given that SRH was storm motion dependent and that BWD and SRH were not perfectly correlated (nor were they independent; not shown), both should be considered. These results for SRH were generally supported by the small Student's *t*-test and MWU *p* values ≤ 0.001, which were supported by medium-to-large effect size indicated by the majority of *d* values ranging from 0.19 to 1.19, with the low of 0.19 for SRH3000 when 30 ≤ PL < 60 mi and 30 ≤ PL < 90 mi were compared to PL ≥ 90 mi and a high of 1.19 for SRH500 when PL < 10 mi was compared to PL ≥ 90 mi. The MWU *f* values ranged from 0.573 to 0.834, and the MWU *r* values ranged from 0.146 to 0.669. The smallest *d*, *f*, and *r* values, all indicating small effect size, were found when comparing pathlength bins with 30 ≤ PL < 60 mi as well as 30 ≤ PL < 90 mi with PL ≥ 90 mi, suggesting that SRH was not as important in distinguishing long-track and very-long-track tornadoes from extremely long-track tornadoes, as SRH was for distinguishing between PL < 30 mi and PL ≥ 90 mi. The SRH500, SRH1000, and SRH3000 distributions were roughly symmetric about their median values with absolute skewness mostly ≤ 0.4 (see supplemental material) except the distributions for PL < 10 mi and PL < 30 mi, which were more skewed to the right with values expectedly more clustered toward smaller values. Recently, Britt et al. (2020) showed observationally and with a warn-on-forecast convection-resolving model (horizontal resolution of 1 and 3 km) that smaller amplitudes of both 10–1000-m SRH and STP (with all else the same, smaller SRH reduces STP) might be indicative of enhanced cyclic supercell mesocyclone behavior in a case study of four storms. Supercell storms with a more cyclic nature that are associated with smaller SRH (Britt et al. 2020) would also suggest shorter longevity and pathlengths for individual tornadoes.

Storm-relative mean-layer inflow kinetic energy (SRMLIKE; based on mean storm-relative inflow squared; m^2 s^{-2}; Fig. 9, bottom row) for the 10–500-m layer also showed discrimination capability between shorter- and longer-track tornadoes, more so than some other wind variables, but with slightly lower R^2 with PL than SRH500. This was consistent with the generally small Student's *t*-test and MWU *p* values; however, the effect size was mostly medium for SRMLIKE as suggested by *d* values generally ≤ 0.81, *f* values from 0.489 to 0.739, and *r* values from −0.021 to 0.478 (small only for intra-long track comparisons). SRMLIKE results were skewed toward the right in most layers and especially so for shorter-track tornadoes; therefore, more weight might be given to the MWU

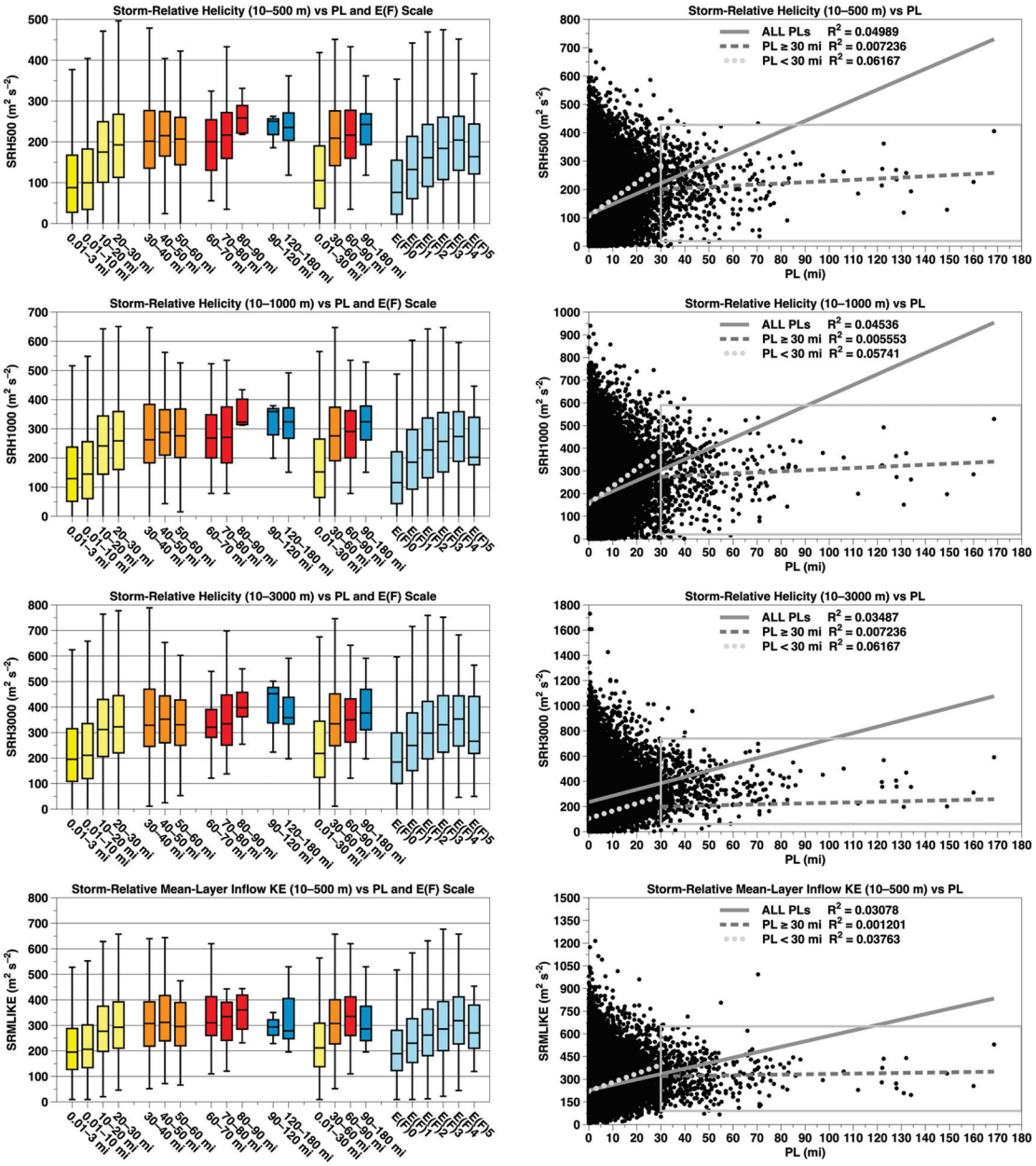

FIG. 9. As in Fig. 1, but for storm-relative helicity (SRH; $m^2\ s^{-2}$) for 10–500, 10–1000, and 10–3000 m, along with storm-relative mean-layer kinetic energy (SRMLIKE; $m^2\ s^{-2}$) for the 10–500-m layer.

statistics. Values of TSS_{max} were largely consistent with other statistics.

The ratio of the mean horizontal streamwise vorticity between 10 and 500 m and mean horizontal streamwise vorticity between 10 and 1000 m and the ratio of the mean horizontal streamwise vorticity between 10 and 1000 m and mean horizontal streamwise vorticity between 10 and 3000 m (Fig. 10) both indicated tornadoes occurred with almost any values of both of these ratios, ranging from $\ll 0$ to $\gg 100$ (negative values can occur), but most occurred within a small range of values. Longer-track tornadoes occurred 97.5% of the time with narrow ranges of these ratios between 0.55–2.17 and 0.74–3.10, respectively, with medians of ~1.4 for the former ratio and ~2.1 for the latter ratio. Perhaps a richer supply of streamwise vorticity, or at least some nominal amount of nearly undiluted inflow streamwise vorticity, indicated by a smaller ratio of mean streamwise vorticity for two layers, is necessary for long-track tornadoes. These results were perhaps relevant given the recent simulations by Peters et al. (2023), who demonstrated that inflow horizontal streamwise vorticity was the "primary control on low-level mesocyclones in sustained supercells" rather than SRH. They are also relevant in the context of studies that considered various horizontal vorticity ratios (C19), streamwise-to-crosswise vorticity ratios (Coffer and Parker 2018), and streamwise percentages (Nixon and Allen 2022).

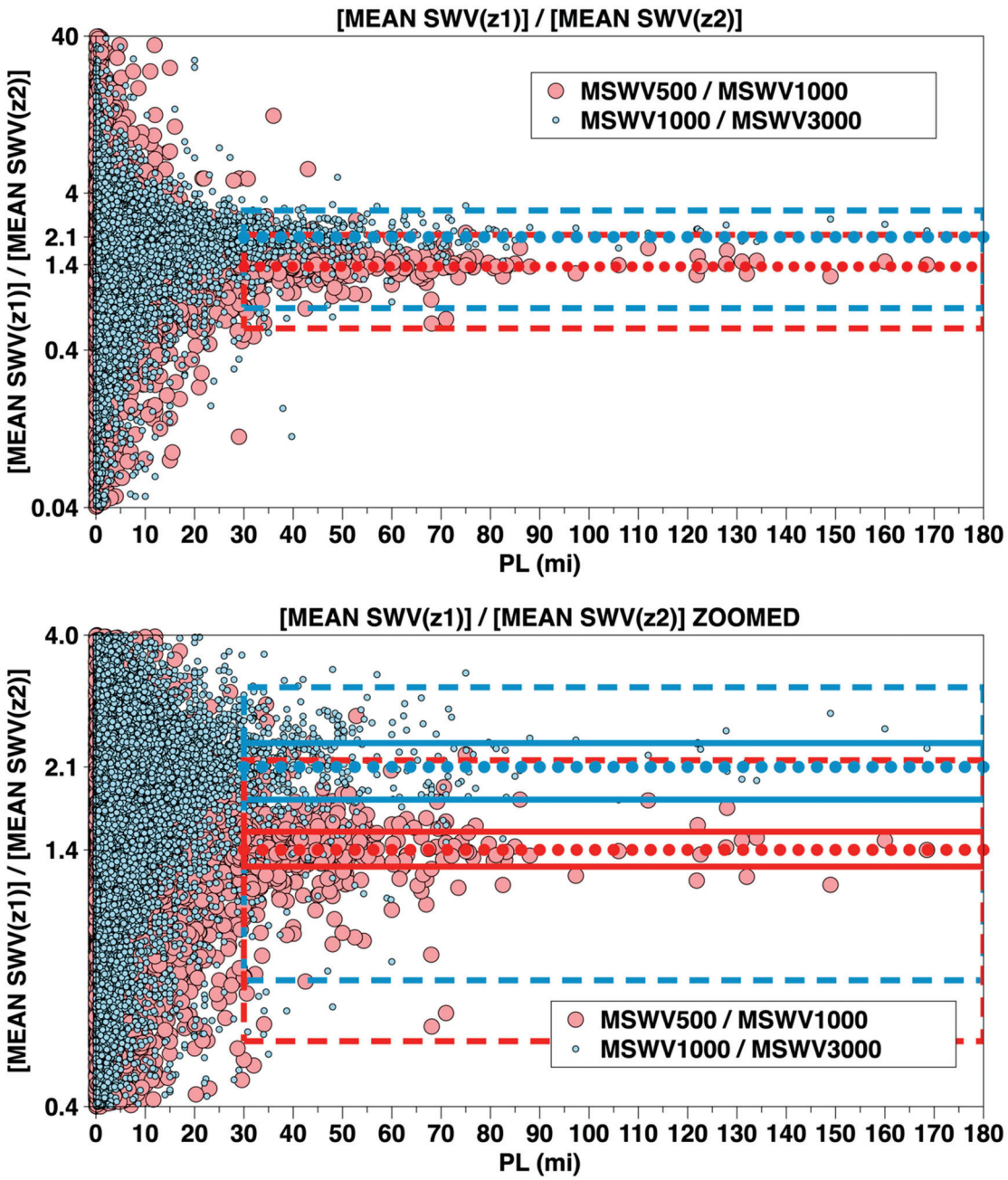

FIG. 10. Scatterplots of the ratio of mean streamwise vorticity between 10 and 500 m (MSWV500) and mean streamwise vorticity between 10 and 1000 m (MSWV1000) plotted using log scale with large light red dots, and mean streamwise vorticity between 10 and 1000 m and mean streamwise vorticity between 10 and 3000 m (MSWV3000) plotted using log scale with small light blue dots. Only ratio values of 0.04–40 are shown in the top plot. The large bold red and blue dotted lines are the median values (Q2 = 1.40 and 2.10) for the ratios of MSWV500/MSWV1000 and MSWV1000/MSWV3000, respectively. For PL ≥ 30 mi, the 2.5th and 97.5th percentiles for the MSWV500/MSWV1000 points lie within the values of 0.55–2.17 (red dashed rectangle), and the 2.5th and 97.5th percentiles for the MSWV1000/MSWV3000 points lie within the values of 0.74–3.1 (blue dashed rectangle). The bottom plot is the same as the top plot but zoomed in for a range of ratio values of 0.4–4; for PL ≥ 30 mi in the bottom plot, the 25th and 75th percentiles for the MSWV500/MSWV1000 points lie within the values of 1.29–1.53 (red solid rectangle), and the 25th and 75th percentiles for the MSWV1000/MSWV3000 points lie within the values of 1.79–2.36 (blue solid rectangle).

Finally, consistent with C19 and G21, critical angles (plots not shown; CA500 statistics in tables) for both larger E(F)-scale rated tornadoes and longer-track tornadoes, respectively, were typically between 40° and 70°, and toward the lower end of this range for longer-track tornadoes, using ERA5 vertical profiles herein, rather than near 90° reported by Esterheld and Giuliano (2008) in their exploratory study relating critical angle and E(F) ratings. Given that the majority of longer-track tornadoes were

associated with higher-end E(F) ratings, one might expect longer-track tornadoes to be associated with critical angles near 90° if Esterheld and Giuliano's results were more general, but longer-track tornadoes were not, with MWU r values and TSS_{max} all indicating an inverse relation between PL and critical angle.

As was the case with the thermodynamic sounding parameters, box-and-whisker plots for all of the kinematic parameters discussed thus far displayed greater interquartile separation between PL bins, while scatterplots appeared to discriminate poorly between PL bins (Figs. 2–9; right column). The R^2 values for linear fits of the kinematic parameters were only slightly better (3.6×10^{-2}–6.8×10^{-2}) than those for the thermodynamic variables (1.3×10^{-6}–1.1×10^{-2}), but unexpectedly better for shorter-track tornadoes with PL $<$ 30 mi than longer-track tornadoes with PL $\geq$ 30 mi for the kinematic variables.

Nevertheless, the scatterplots showed that while tornadoes with PL $<$ 30 mi, as well as with almost any E(F) scale, can be found with most any tropospheric wind speeds and associated wind parameters, there seemed to be a lower bound, approximated by the rectangles on the scatterplots, on these variables for tornado PLs $\geq$ 30 mi, especially for values of wind speeds and BWDs above 4000 m, and for surface storm-relative winds, but not evident for values of SRH. This finding was more profound for all wind speeds and bulk wind differences at all levels for tornado PLs greater than about 80 mi. The lower bound was likely associated with faster-moving parent storms with long-track tornadoes (Fig. 5). It was not clear, however, whether the lack of a better-defined lower bound of SRH with longer-track tornadoes was associated with poor sampling of the actual wind profile in the ERA5 datasets, which is quite possible given that the ERA5 model has a horizontal grid spacing of ~30 km. Markowski et al. (1998a,b,c) and Rasmussen et al. (2000) all showed considerable variability in time (<1 h) and space (<few kilometers) in observed soundings from tornadic storm environments, especially near various surface boundaries. These studies showed the above statements also might hold true for many of the ERA5 kinematic or thermodynamic vertical profile attributes. Finally, the scatter diagrams show that there was not much distinction in individual variables for tornadoes with PL $\geq$ 60 mi. It is quite possible that various factors such as associated storm interactions and mesoscale inhomogeneities might become increasingly relevant for the very-long-tornado PLs, or perhaps the number of very-long-track tornadoes was too small to provide meaningful results.

In summary, kinematic parameters, like thermodynamic parameters, used here also were not particularly useful to uniquely indicate tornado pathlength using the methods employed herein but were helpful to discern generally between shorter and longer tornado PLs. However, weaker wind values below specific thresholds at any, some, or all of the low, mid, and upper levels excluded the possibility of long-track tornadoes. Finally, TSS_{max} values for kinematic variables generally indicated the same relative degree of importance as other statistics, with the largest TSS_{max} values for PL $<$ 10 mi compared to PL $\geq$ 90 mi, followed by 60 $\leq$ PL $<$ 90 mi, 30 $\leq$ PL $<$ 90, PL $\geq$ 30 mi, and PL $<$ 30 mi compared to PL $\geq$ 30 mi.

c. *Composite sounding parameters*

There has been much historical and present interest in the development of composite parameters from sounding and reanalysis vertical profile data to diagnose severe convective weather environments that might favor hail, strong winds, and tornadoes (Johns et al. 1993; T03; Gensini et al. 2021). Larger values for STPcin500, STPcin1000, VTPcin500, and EHI500 (Fig. 11; Table 2; note, variables in Fig. 11 with SRH500/75, for example, means SRH500 divided by 75 m^2 s^{-2}) were found for longer tornado pathlengths, especially for PL $\geq$ 80 mi, as well as for higher E(F)-rated tornadoes, with the latter as expected based on most previous studies (e.g., T03; T20a). Furthermore, as shown earlier, longer-track tornadoes (especially for PL $\geq$ 70 mi) and more significant tornadoes [especially for >E(F)3] were both associated with larger values of CAPEml and CAPEmu, with occasionally smaller values of CINml, and lower values of LCLml for some longer PL bins. Similarly, larger values of low-, mid-, and upper-level wind speed and bulk wind speed differences, storm-relative surface wind speeds, and SRHs were associated with longer-track tornadoes and larger E(F)-scale ratings. Hence, the overlap of the middle 50% values for STPcin500, STPcin1000, VTPcin500, and EHI500 among the PL bins was not unexpected and perhaps due to the overlap of CAPEml, CINml, LCLml, SRH500, BWD at 6000 m (BWD6000), etc. However, there was slightly less overlap for E(F)-scale bins, for which, at least in part, STPcin500, STPcin1000, and VTPcin500 were developed {i.e., STPcin500 for delineation of weaker [E(F)0–1] from significant tornado [E(F)2–5] environments and VTPcin500 for delineation of violent tornado [E(F)4–5] environments}. Scatterplots showed markedly little trend for any of these composite parameters vs PL, with the STPcin500 having the highest R^2 for a linear fit. Moreover, the whiskers for STPcin500, STPcin1000, VTPcin500, and EHI500 for the PL bins and the E(F)-scale bins almost all extend to near zero; some of these very low values were likely due to inaccurate model sampling of the true atmosphere as discussed earlier (this might be less of an issue with high-resolution, convection-permitting models; Britt et al. 2020). Nevertheless, the Student's t-test p values and associated d values generally indicated statistical significance with $p \leq 0.001$ and medium-to-large effect size for STPcin500, STPcin1000, and EHI500 and less so for VTPcin500, respectively, for indicating longer-track tornadoes in most bin comparisons. Similar statistical results for STPcin500, STPcin1000, and EHI500 were found using MWU p values $<$ 0.001, which were supported with medium-to-large effect size based on f values and r values to indicate longer-track tornadoes, and less so for VTPcin500. The distributions for these composite scores were notably right skewed with skewness $>$ 0.6 (see supplemental material) for almost all PL bins, except for PL $\geq$ 90 mi, for which they were more symmetric. Therefore, more weight might be given to interpretation based on the MWU statistics. Finally, TSS_{max} scores were larger for STPcin500, STPcin1000, and EHI500 than for VTPcin500 and VTPcin1000 (latter in the supplemental material); however, only a few comparisons between PL bins produced $TSS_{max} \geq 0.4$ (comparisons of PL $<$ 10 with

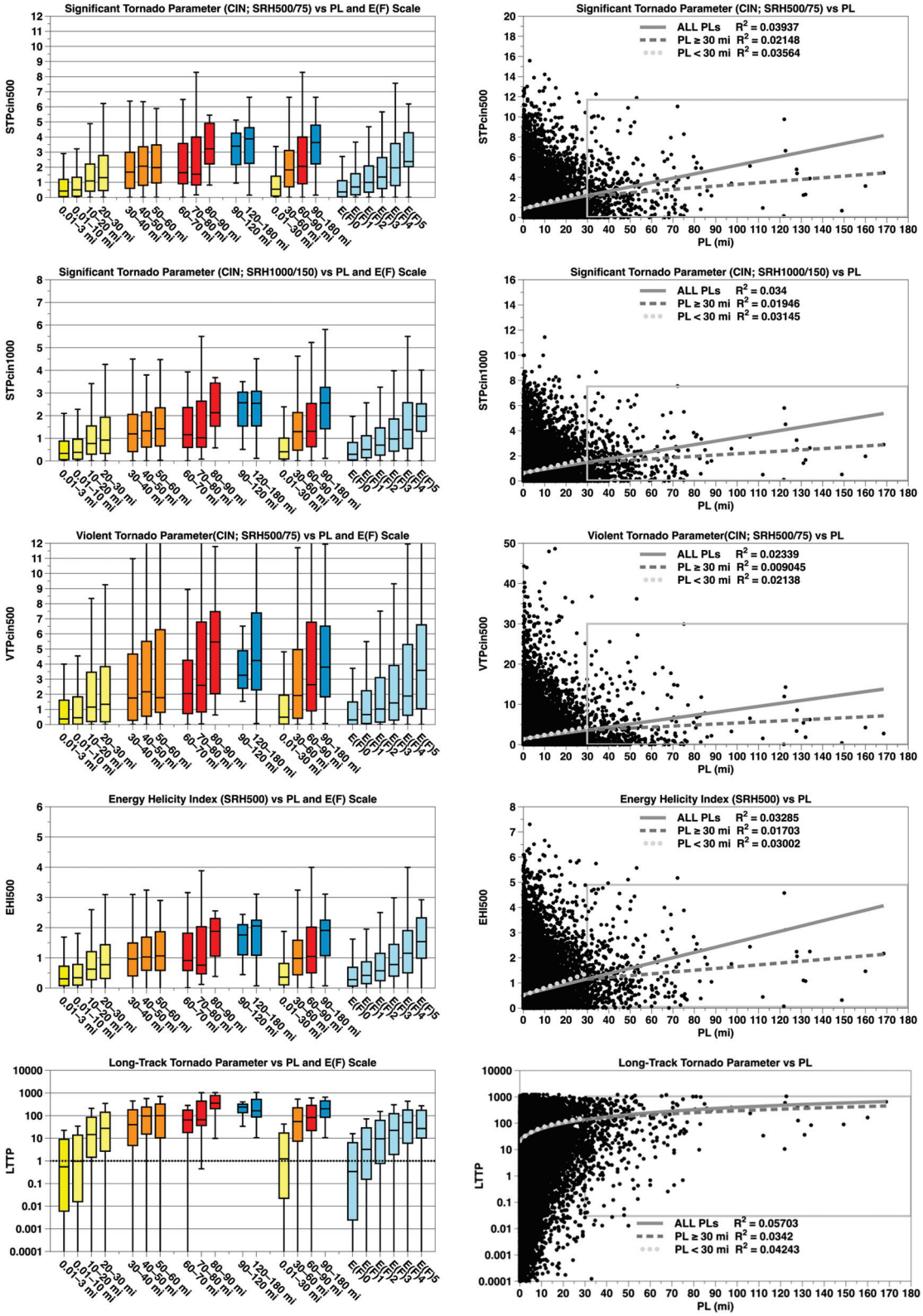

FIG. 11. As in Fig. 1, but for STPcin500, STPcin1000, VTPcin500, EHI500, and LTTP.

$60 \leq PL < 90$ mi and $PL \geq 90$ mi), and even fewer reached medium forecast skill with $TSS_{max} \geq 0.6$ {(e.g., comparisons of $PL < 10$ with $PL \geq 90$ mi), also for E(F)-scale comparisons [<E(F)5 with E(F)5] shown in the supplemental material as well as by C19 comparing right moving supercells with E(F)2+ tornadoes, E(F)0−1 tornadoes, and nontornadic storms with significant wind and/or hail and no nearby tornadoes within 185 km and 3 h, for example}.

5. Long-track tornado parameter

Parameters developed previously to identify supercells such as bulk Richardson number (BRN; Weisman and Klemp 1982; 1984), supercell composite parameter (SCP) (T03; T07), and EHI (Hart and Korotky 1991); for supercells with and without tornadoes (none, weak, significant, and violent tornadoes), EHI, STP, and VTP (e.g., R03, T03; T07) are routinely used by weather forecasters to help delineate and diagnose areal coverage of severe weather threats and intensities. A shortcoming of these composite parameters includes the issue of how mutually independent each parameter is from the other parameters.

A question is, "can the use of thermodynamic and wind parameters, perhaps differently weighted than in the STP, VTP, and EHI, provide better discrimination between environments more often associated with longer-track tornadoes than those associated with shorter-track tornadoes?" In the spirit of the development of STP, a long-track tornado parameter (LTTP) was developed, with the same caveats as other severe weather parameters. The LTTP was developed using thermodynamic parameters (CAPEml, LCLml, and CINml) and kinematic parameters (maximum wind speed from 200 to 2000 m for low levels, wind speed at 4000 m for midlevels, maximum wind speed from 5000 to 9000 m for upper levels, storm-relative surface wind speed, 10–500-m BWD, 10–4000-m BWD, and maximum 10-m to 5000–9000-m BWD).

Clearly, most of these parameters were not entirely independent, nor were they entirely dependent. Shorter-track tornadoes were often associated with smaller wind speeds and shears at only some of the lower, mid, and upper levels, compared to longer-track tornadoes, which had larger values at all of these levels, especially for the longest-track tornadoes. Therefore, while there is some dependence on kinematic variables at low, mid, and upper levels, they all had to be larger for longer-track tornadoes. If one or more were too weak, the multiplicative impact reduced (penalized) the LTTP values accordingly.

Results for the LTTP with the low-, mid-, and upper-level wind parameters as indicated above produced slightly better results than using wind speed and BWD (from 10 m) for 1000, 1500 m, or 850 mb for the low levels; 2000 or 3000 m for the midlevels; and 5000, 6000, 7000, 8000, 9000, or 10 000 m for the upper levels. Also, guided by C19, we use SRH500 rather than using other depths including 10–1000, 10–2000, 10–3000, 0–4000, or 0–6000 m, all of which were less (often much less such as with SRH from 0 to 6000 m) statistically robust than using SRH from 0 to 500 m. Extensive statistical measures of these individual wind variables are provided in the appendices and supplemental materials as discussed earlier. Note that changing the height for wind variables used at the lower, mid, and upper levels as described above did not appreciably change any conclusions as long as some representations for these were all used. This is discussed further below.

The nondimensional LTTP equation, in pseudocode, is given by

$$\text{LTTP} = (\text{LTTPt} \times \text{LTTPk})/(\text{Fn}),$$

where the thermodynamic term (LTTPt) contains the thermodynamic-related terms, the kinematic term (LTTPk) contains the kinematic-related terms, and Fn = 33.71 is a factor to normalize the results (as well as remove dimensions), such that a value of LTTP = 1 corresponds to the median LTTP for tornado pathlengths in the range of $0.01 \leq PL < 10$ mi.

The components of thermodynamic terms in the proposed LTTP have a similar form as those in STP, with the CAPEml and LCLml terms modified to better represent long-track tornado potential. Specifically, CAPEml was normalized by the Q1 value of CAPEml (J kg^{-1}) for $0.01 < PL \leq 10$ mi instead of 1500 J kg^{-1}, as done with the STP, and limited to a maximum normalized value based on the Q3 value of CAPEml for $60 \leq PL < 90$ mi. Next, LCLml was normalized by 700 m instead of 1000 m as in the STP, with a maximum LCL of 2100 m rather than 2000 m as in the STP. Values of CINml were used in the same manner in the STP. The forms of the specific terms in the LTTPt term are given as

$$\text{LTTPt} = \text{tcape} \times \text{tlcl} \times \text{tcin},$$

where

$$\text{tcape} = \max\{\min[\text{CAPEml}/319.23), (1534.88/319.23)], 0.0\};$$

$$\text{tlcl} = \min\{\max[(2100.0 - \text{LCLml})/1400.0, 0.0], 1.0\};$$

with tlcl = 0, if LCLml ≥ 2100.0 m, and tlcl = 1, if LCLml ≤ 700.0, and

$$\text{tcin} = \min\{\max[(200.0 - \text{CINml})/150.0, 0.0], 1.0\}.$$

The kinematic term was developed by normalizing each parameter by its Q1 value from the $0.01 \leq PL < 10$-mi PL bin values and limited by its Q1-normalized Q3 values for the $60 \leq PL < 90$-mi bin values; i.e., max {min[ϕ/ϕ(Q1), ϕ(Q3)/ϕ(Q1)], 0.0}, where ϕ is some parameter. The kinematic parameters used in the LTTP were chosen based on the highest normalized values of SRH (500, 1000 … 6000 m), SRMLIKE (500, 1000 … 6000 m), storm-relative wind speed (surface, 500, 1000 … 9000 m), and highest normalized values for wind speeds and BWD low levels ($200 \leq z < 2000$ m or max), midlevels ($2000 \leq z < 5000$ m), and upper levels ($5000 \leq z < 9000$ m or max) based on comparisons of both $PL < 10$ mi compared with $PL \geq 30$-mi results and $PL < 30$ compared with $PL \geq 30$-mi results. The use of this procedure

is supported with the Student's *t*-test *p* values and corresponding Cohen's *d* values for effect size (as well as TSS_{max} and MWU *p* values, *f* values, and *r* values). The forms of the specific terms in the LTTPk term are given as

$$\begin{aligned}\text{LTTPk} = {} & \max\{\min[(\text{SRH500}/35.26), (277.24/35.26)], 0.0\} \\ & \times \max\{\min[(\text{SRWSSFC}/10.99), (24.22/10.99)], 0.0\} \\ & \times \max\{\min[(\text{SRMLIKE}/134.99), (411.86/134.99)], 0.0\} \\ & \times \max\{\min[(\text{BWD500}/4.63), (14.45/4.63)], 0.0\} \\ & \times \max\{\min[(\text{BWD4000}/14.23), (30.46/14.23)], 0.0\} \\ & \times \max\{\min[(\text{BWDULMAX}/20.91), (43.21/20.19)], 0.0\} \\ & \times \max\{\min[(\text{WSLLMAX}/12.00), (28.75/12.00)], 0.0\} \\ & \times \max\{\min[(\text{WS4000}/14.99), (34.04/14.99)], 0.0\} \\ & \times \max\{\min[(\text{WSULMAX}/21.64), (46.47/21.64)], 0.0\}.\end{aligned}$$

These vertical profile parameters (defined in Table 2), of all considered, were found to provide the robust Student's *t*-test *p*-value results ($\leq$0.001; as well as MWU *p* values $\leq$ 0.001) after extensive experimentation with various combinations.

For reference, the limiting normalized minima for each variable were zero, while the limiting normalized maxima for each variable (maximum quantities in the normalized terms above) are provided in Table 3. The five heaviest-weighted components, i.e., those with the largest normalized maxima, include SRH500, CAPEml, BWD500, SRMLIKE, and WSLLMAX, and these values are shown in bold numbers in Table 3).

Values of LTTP (Fig. 11) show substantial spread for tornadoes with PL $<$ 10 mi to PL $\geq$ 90 mi. The biggest percentage changes in Q1, Q2, and Q3 values for LTTP occurred among the shorter PL comparisons, with lesser changes for longer PL comparisons. Some of the largest percentage changes were for 0.01 $\leq$ PL $<$ 30 mi compared to 30 $\leq$ PL $<$ 60 mi for not only LTTP but also STP, VTP, and EHI. The values of LTTP were notably skewed to the right, with values clustered toward smaller values. Ratios of Q1, Q2, and Q3 values of all PL stratifications to Q1, Q2, and Q3 values for 0.01 $\leq$ PL $<$ 10 mi compared to those from EHI, STP, or VTP indicated that the LTTP has more potential for discriminating shorter-track ($<$30 mi) tornadoes from longer-track ($\geq$30 mi) tornadoes when values for LTTP were above either the lower- or midquartile values for the PL $\geq$ 30-mi bins. Both shorter-track and longer-track tornadoes were associated with wide ranges of LTTP values, with longer-track tornadoes more notably associated with larger values at Q1, Q2, and Q3 than shorter-track tornadoes and shorter-track tornadoes more associated with Q2 values that were often more than 10 times smaller for the medians than those for those for longer-track tornadoes. Importantly, *p* values $<$ 0.001 for most PL bin comparisons support these findings when comparing shorter-track tornado PL bins to longer-track tornado PL bins, but not as much for intercomparisons of longer-track tornado PL bins, such as 30–60 mi or 30–90 mi with $\geq$90 mi, which had somewhat larger *p* values of 0.019 and 0.037, respectively. Additionally, mostly large effect sizes were found for the LTTP (0.58–3.08) and the kinematic component LTTPk (0.39–1.62) when comparing shorter- and longer-track tornadoes, with corresponding effect sizes generally being much smaller for the thermodynamic component LTTPt (0.15–0.84), which was consistent with kinematics showing more importance than thermodynamics to indicate tornado PL. Note that LTTPt and LTTPk are not normalized before statistics are computed.

TABLE 3. Limiting normalized maximums for each variable in the LTTP parameter. The five largest values are indicated in bold.

Parameter	Maximum normalized value
CAPEml	**4.81**
LCLml	1
CINml	1
SRH500	**7.86**
SRWSSFC	2.20
SRMLIKE	**3.05**
BWD500	**3.12**
BWD4000	2.14
BWDULMAX	2.07
WSLLMAX	**2.4**
WS4000	2.27
WSULMAX	2.15

Favorable and comparable statistical results were found for both STPcin500 and LTTP results using MWU, with *f* values (*r* values) ranging from 0.658 to 0.858 (0.315–0.715) for the former and from 0.695 and 0.930 (0.390–0.860) for the latter. These indicate that the LTTP performed better than STP500, and from the tables, LTTP performed better than any of the discussed composite parameters. Values of TSS_{max} also support that LTTP could better distinguish PL than STPcin500 [TSS_{max}(LTTP) = 0.320/0.466/0.760/0.445 compared to TSS_{max}(STPcin500) = 0.242/0.361/0.658/0.347 for PL $<$ 10 vs PL $\geq$ 10 mi/PL $<$ 10 vs PL $\geq$ 30 mi/PL $<$ 10 vs PL $\geq$ 90 mi/PL $<$ 30 vs PL $\geq$ 30 mi; see supplemental table for all TSS_{max} values]. Finally, LTTP better distinguished between tornado E(F)-scale ratings for ratings less than E(F)5 [TSS_{max} for E(F) scale not shown but is provided in the supplemental material] than STPcin500 [TSS_{max}(LTTP) = 0.249–0.424 and TSS_{max} (STPcin500) = 0.183–0.382, respectively], while STPcin500 better distinguished between E(F)5 and E(F)0–4 rated tornadoes than LTTP [TSS_{max}(LTTP) = 0.467 and TSS_{max}(STPcin500) = 0.613, respectively], perhaps owing to the lesser impact of CAPEml on LTTP than on STP. Interestingly, EHI500 and EHI1000, but not EHI3000, outperformed or performed as well as STPcin500 or STPcin1000 to distinguish tornadoes rated E(F)4+, especially E(F)5 tornadoes, from weaker rated tornadoes [e.g., TSS_{max}(EHI500) = 0.416 and 0.611 and TSS_{max}(STPcin500) = 0.382 and 0.613, respectively], while the VTP performed the least favorably [TSS_{max}(VTPcin500) = 0.293 and 0.433]. Importantly, none of LTTP, STPcin500, STPcin1000, VTPcin500, or EHI500

TABLE 4. Values of TSS_{max} for LTTP, with one or more parameters changed or removed and relative percent changes from LTTP in parentheses below values of TSS_{max}. A positive (negative) relative percent change means skill, based on TSS_{max}, for LTTP was increased (decreased) when one or more parameters were changed or removed, with TSS_{max} values of 0.2–0.6, 0.6–0.8, and ≥0.8 indicating low, medium, and high forecast skill. Italicized values indicate the change increased (decreased) TSS_{max} by 2.5%–5% compared to the TSS_{max} for the proposed LTTP, and bold, italicized values indicate the change was ≥5%. Acronyms are WS for wind speed, BWD for bulk wind difference, and SRWSSFC, SRH500, and SRMLIKE500 are as defined in Table 2.

TSS_{max} (percent relative difference from LTTP)	<10 30–60	<10 30–90	<10 60–90	<10 ≥30	<10 ≥90	<10 ≥10	<30 >30	<60 ≥60	<90 ≥90
LTTP	0.442	0.459	0.572	0.466	0.760	0.320	0.445	0.575	0.739
WS500, BWD500, BWD9000	0.448 (1.4)	0.460 (0.02)	*0.556* *(−2.8)*	0.467 (0.21)	0.755 (−0.66)	0.317 (−0.94)	0.446 (0.22)	0.573 (−0.35)	0.734 (−0.68)
No BWD (all levels)	0.446 (−0.90)	0.459 (0.0)	0.566 (−1.0)	0.465 (−0.21)	*0.733* *(−3.6)*	0.315 (−1.6)	0.445 (0.0)	0.571 (−0.70)	*0.710* *(−3.9)*
No WS (all levels)	0.437 (−1.1)	0.449 (−2.2)	***0.539*** ***(−5.8)***	0.455 (−2.4)	*0.729* *(−4.1)*	***0.304*** ***(−5.0)***	0.435 (−2.2)	***0.544*** ***(−5.4)***	*0.708* *(−4.2)*
No lower-level BWD or WS	0.437 (−1.1)	0.453 (−1.3)	0.584 (2.1)	0.460 (−1.3)	*0.728* *(−4.2)*	*0.308* *(−3.8)*	0.440 (−1.1)	0.570 (−0.87)	*0.709* *(−4.1)*
No middle-level BWD or WS	0.440 (−0.45)	0.454 (−1.1)	*0.556* *(−2.8)*	0.459 (−1.5)	*0.741* *(−2.5)*	*0.312* *(−2.5)*	0.438 (−1.6)	0.561 (−2.4)	*0.720* *(−2.6)*
No upper-level BWD or WS	0.436 (−1.5)	0.448 (−2.4)	***0.537*** ***(−6.1)***	0.456 (−2.1)	***0.715*** ***(−5.9)***	0.314 (−1.9)	0.435 (−2.2)	***0.541*** ***(−5.9)***	***0.691*** ***(−6.5)***
Only lower-level BWD and WS	***0.419*** ***(−5.2)***	***0.430*** ***(−6.3)***	***0.508*** ***(−11.2)***	***0.436*** ***(−6.4)***	***0.708*** ***(−5.5)***	***0.300*** ***(−6.3)***	***0.415*** ***(−6.7)***	***0.505*** ***(−12.2)***	***0.688*** ***(−6.9)***
Only middle-level BWD and WS	***0.419*** ***(−5.2)***	***0.430*** ***(−6.3)***	***0.543*** ***(−5.1)***	***0.435*** ***(−6.7)***	***0.682*** ***(−10.3)***	***0.301*** ***(−5.9)***	***0.416*** ***(−6.5)***	*0.548* *(−4.7)*	***0.659*** ***(−10.8)***
Only upper-level BWD and WS	*0.422* *(−4.5)*	***0.436*** ***(−5.0)***	***0.532*** ***(−7.0)***	***0.442*** ***(−5.2)***	***0.691*** ***(−9.1)***	***0.296*** ***(−7.5)***	*0.423* *(−4.9)*	***0.530*** ***(−7.8)***	***0.671*** ***(−9.2)***
No SRWSSFC	0.440 (−0.45)	0.455 (−0.87)	0.573 (0.17)	0.461 (−1.1)	0.747 (−1.7)	0.320 (0)	0.439 (−1.3)	0.564 (−1.9)	0.725 (−1.9)
No SRH500	0.449 (1.6)	0.470 (2.4)	***0.610*** ***(6.6)***	0.476 (2.1)	0.756 (−0.53)	0.316 (−1.3)	0.456 (2.2)	*0.600* *(4.3)*	0.735 (−0.54)
No SRMLIKE500	0.444 (0.45)	0.463 (0.87)	*0.600* *(4.9)*	0.471 (1.1)	*0.781* *(2.7)*	0.315 (−1.6)	0.449 (1.1)	*0.597* *(3.8)*	*0.760* *(2.8)*
No SRH500, no SRMLIKE500	*0.459* *(3.8)*	*0.480* *(4.6)*	***0.620*** ***(8.3)***	*0.486* *(4.3)*	*0.781* *(2.7)*	*0.312* *(−2.5)*	*0.466* *(4.7)*	***0.606*** ***(5.4)***	*0.766* *(3.7)*
No thermodynamic component in LTTP	0.445 (0.68)	0.453 (−1.3)	*0.551* *(−3.7)*	0.462 (−0.86)	0.745 (−2.0)	0.322 (0.63)	0.442 (−0.67)	*0.556* *(−3.3)*	0.725 (−1.9)

were associated with high forecast skill (e.g., $TSS_{max} > 0.8$) for PL or E(F)-scale rating.

Keeping in mind that the proposed LTTP was based on parameter values based on normalized Q1 associated with 0.01 ≤ PL < 10-mi values and limited by the normalized maximum Q3 associated with 60 ≤ PL < 90-mi values, comparisons between 14 variations (not exhaustive) of LTTP (besides the one proposed), with one or more variables changed or removed, are shown in Table 4. Quite unexpectedly, removing SRH500 and/or SRMLIKE500 generally increased TSS_{max} by 0.45%–6.6% compared to the proposed LTTP, with the greatest changes (>5%) when comparing PL bins where one had a PL ≥ 60 mi, but not always. Removing SRH500 and/or SRMLIKE500 decreased TSS_{max} only when comparing PL < 10 mi to PL ≥ 10 mi. When all BWD values, all wind speed (WS), storm-relative WS at surface (SRWSSFC) values, or any combination of conditions when one or two levels of both BWD and WS values together were removed, values of TSS_{max} mostly decreased (i.e., 0.0% to −11.2%) compared to the proposed LTTP. The removal of SRWSSFC, with all else the same, had the least overall impact (decrease) on values of TSS_{max}, while using only lower-level BWD and WS of the levels used in the LTTP, with all else the same, had the largest overall impact (decrease). Furthermore, the greatest generally negative impact on TSS_{max} when changing or removing one or more parameters occurred when only one level for BWD and WS was used. Finally, removing the thermodynamic component decreased TSS_{max} values by >5% when one of the bins in a comparison was PL ≥ 60 mi or 60 ≤ PL < 90 mi; otherwise, the impact was ≤0.68%.

6. Summary

Environmental synthetic proximity soundings from ERA5 reanalysis data for all tornadoes with a PL ≥ 0.01 mi over the CONUS between 1979 and 2022 were examined in the context of short, long, very-long, and extremely long-tornado tracks. No one thermodynamic or kinematic quantity robustly provided definitive forecast/diagnostic guidance for long-track tornadoes. Rather, this study showed that environments that support long-track tornadoes were also consistent with those that support stronger- and faster-moving supercells.

Some findings, from a thermodynamic point of view, were that long-track tornadoes, like stronger tornadoes, preferentially formed in environments with adequate CAPEml (500–1500 J kg^{-1}) for vigorous deep convection, but not necessarily extremely large values of CAPEml. Importantly, LCLml heights above 1200 m were not often found with long-track tornadoes or higher E(F)-scale rated tornadoes. Murdzek et al. (2024) recently showed higher LCL heights in simulations are more likely to produce cold surges that could disrupt tornado maintenance. Values of CAPE03ml, LCLml, and CINml were not particularly useful in discriminating between shorter- and longer-track tornadoes. As mentioned earlier, the requirements of at least some CAPEml, a low LCLml, and CINml that was not too large might only be conditions for deep, vigorous, moist convection and not necessarily for tornadic convection.

In contrast to the thermodynamic parameters, kinematic parameters overall showed greater and more consistent statistical association with longer tornado PLs. The strongest associations for PL at heights below 2000 m were with SRH, BWD, and surface storm-relative winds. These signals were often also associated with strong rotational characteristics in the low levels of supercells. There was also a long-track tornado signal associated with strong wind speeds from 4000 to 9000 m, as well as with stronger wind speeds from 10 to 2000 m. Stronger mid- to upper-level wind speeds were expectedly well correlated with faster Bunkers' ID storm speed. Additionally, BWDs between 10 m and any level between 500 and 10 000 m also provided PL discrimination. A large (roughly 15%–40%) portion, but nonmajority, of the hodograph length associated with tornadic storms in general, especially with longer-track tornadoes, was between 10 and 1000 m. In dramatic contrast to the lower levels, larger values of storm-relative wind speeds at and above 6000 m often were sometimes negatively associated with longer-track tornadoes, albeit slightly, with smaller upper-level BWDs between, for example, 6000 and 9000 m rather than between 10 and 3000 m. The weak signal with flow/shear above 6000 m might just be more likely to exist in the atmosphere than at levels ≤6000 m, rather than to be supportive of tornadic supercells and the PLs of tornadoes they produce.

We debated the development of a LTTP as the following quote from B06 seemed particularly relevant, "a single parameter belies the importance of all other potentially relevant characteristics of the mesoscale to synoptic scale environment, and could possibly mislead a forecaster into making an incorrect assessment of supercell longevity." Nevertheless, we proceeded and found that the LTTP outperformed the various STPs for distinguishing both PL and most E(F)-scale comparisons. Other composite parameters that showed PL discrimination were the various EHIs and VTPs, interestingly, while EHI500 outperformed or as well as the various STPs for discerning E(F)4+ tornadoes from lower E(F)-rated tornadoes.

All severe weather composite indices considered, including the different variants of STP, VTP, EHI, and LTTP, showed statistical significance at $p \leq 0.001$ for both the Student's t test and the MWU, with medium-to-large effect size support based on d, f, and r values, for all tornado PL bin comparisons, except when both bins being compared had a minimum PL ≥ 30 mi or more (e.g., 30 ≤ PL < 60 mi compared to PL ≥ 90 mi) using the Student's t test, but not using MWU statistics. Moreover, any given composite parameter using 0–500-m SRH always outperformed the same composite parameter using 0–1000-m SRH, as well as that for 0–3000-m SRH in the EHI parameter, in agreement with C19 and Rasmussen (2003) for EF2+ tornadoes compared to occurrences of severe weather. All parameters had high false alarm rates (not shown), echoing the concerns raised by B06, but recall T03 and T07 argued higher false alarm rates were preferred in the forecasting arena, at least with STP, in order to not miss important events.

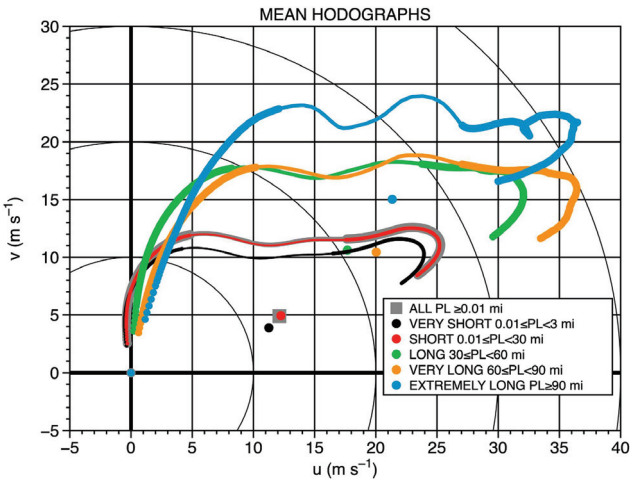

FIG. 12. Mean hodographs based on ERA5 vertical wind profiles for various tornado PLs. The parts of the hodographs in the first 1000 m are denoted with bolder lines, as are the parts of the hodographs from 6000 to 14 000 m, while parts of the hodograph between 1000 and 6000 m are denoted with thinner lines. The mean Bunker's ID storm motion velocities for each hodograph are indicated by bold dots off the hodograph with units of m s^{-1}.

Limitations of this study include inaccuracies in reported tornado PLs and reanalysis vertical profiles that do not always accurately represent the true atmospheric conditions; vertical profiles do not account for storm–storm and storm–boundary interactions, and only one time and one location for the reanalysis vertical profile was used. Some of the longest-lasting tornadoes lasted up to ~3 h and the longest path tornadoes had PL > 150 mi, but these extremes comprised a small number of cases. Time-of-day variations (see SK22) were not considered (e.g., CAPEml can be quite a bit lower and low-level shear and SRH can be quite a bit larger), with some notable very strong/violent long-track tornadoes occurring well after dark (e.g., EF4 81+-mi, EF3 122+-mi, and EF4, 168+-mi tornadoes on 10 December 2021 in Tennessee and Kentucky) and some after midnight (e.g., F5 36-mi tornado on 8 June 1984 in Wisconsin). Finally, the evolution, maintenance, and demise of tornadoes are likely related to subtle variations in otherwise broadly tornado-supportive environmental conditions, with the latter almost certainly essential for a tornado to be maintained over a long track. Importantly, these subtle variations cannot be resolved with spatial resolutions of ~30 km and temporal resolutions of 1 h

in the ERA5 data. As C19 note, the use of HRRR resolution data might be useful, but even this would be limited for detecting subtle environmental and storm-scale variations (as well as storm interactions) in the atmosphere that could be relevant to long-track tornadoes. An important question might be to what degree that environment can change and still support an ongoing tornado, which is beyond the scope of this paper.

Pragmatically, forecasts of tornado PLs using vertical profile attributes, perhaps, are not so much a problem of when to have higher expectations for long-track tornadoes, but rather a problem of when to have lower expectations for long-track tornadoes. For example, with weak flows and smaller values of most associated kinematic attributes through the troposphere, especially at, or below, 2000 m, it seems probable that tornadoes do not last long enough and/or translate fast enough to become long-track tornadoes (mean hodographs for various PLs shown in Fig. 12). However, even with strong flow, other factors are required for long-track tornadoes. Importantly, the results herein provide further motivation to better anticipate mesocyclone periodicity, in the context of the association of duration and PL, as this could provide guidance for diagnosing environments most supportive of long-track tornadoes.

Acknowledgments. Gensini was supported by the National Science Foundation (Award AGS-2048770). We thank the Dr. Brice Coffer and two anonymous reviewers for their exceptionally insightful and helpful comments, which led to many improvements in the manuscript. Tom and Doris Grazulis provided helpful discussions and information on several long-track tornado cases during the course of this study. The first author is grateful for past discussions on long-track tornadoes with Drs. R. Davies-Jones, M. Karpovich, A. Kennedy, E. Rasmussen, and L. Reames. Graphics were produced with DataGraph, with special thanks to Pamela Schultz for software assistance with the box and whisker plots.

Data availability statement. Hail and tornado report data are open source and can be obtained from https://www.spc.noaa.gov/wcm/. The ERA5 data were downloaded from the European Centre for Medium-Range Weather Forecasts (ECMWF) and Copernicus Climate Change Service (C3S) available at https://cds.climate.copernicus.eu/. All analysis source codes and associated input statements to process SPC and ERA5 datasets are available from the authors.

APPENDIX A

Two Tornado Cases with Erroneous Pathlengths Removed from the SPC Database for This Study

The following two extremely long-track tornadoes were removed from the database before the algorithmic filter was applied.

1) A narrow and weak, 99.8-mi PL, 40-yd-wide, F1 tornado, on 15 May 1980 in Texas was removed from the SPC tornado dataset based on persistent prestorm and storm time (2315–0200 UTC) ~1–3-km mean winds of ~4.4 m s^{-1}, ~0–6-km mean winds of ~11.7 m s^{-1}, and up to ~2810-m LCLml height (ERA5 vertical profile and Del Rio, Texas, KDRT, 0000 UTC NWS rawinsonde data). The ~30 m s^{-1} 0–6-km bulk shear supported an observed storm motion of ~36 mph meaning the tornado would have persisted for ~166 min. Furthermore, the NCEI *Storm Data* publication (late reports May 1980 in the June 1980 issue) reports "four," but lists five short-lived tornado tracks pathlengths of 1, 8, 2, 1/2, and 1 mi; path widths of 30, 50, 50, 50, and 50 yd; and start times of 2315, 2330, 0040, 0115, and 0200 UTC; none caused property damage or injuries as indicated by *Storm Data*; language in *Storm Data* includes the phrases "probably passed aloft," "before touching the ground again briefly," and "The tornado remained small although long lived, [maximum length of segments reported was only 8 mi] and it touched ground probably four separate times through sparsely populated areas." The storm, which was tracked on radar by the NWS, produced up to 1.75-in. hail that caused crop and property damage. Along-track ERA5 vertical proflies (very weak 0–3-km shear < 7.5 m s^{-1}, weak SRH500 from ~ -70 to 50 m^2 s^{-2}, SRH1000 from ~ -10 to 150 m^2 s^{-2}, and LCLml of ~1200–2800 m) do not support a long-lived tornado as described recently by G21 {their top 50 [≥60 min duration; median SRH1000 = 405 m^2 s^{-2}/standard deviation (SD) 202 m^2 s^{-2} and median LCLml = 747 m/SD 310 m] and top 25% (312 events; 20–138 min durations; median SRH1000 336 m^2 s^{-2}/SD 197 m^2 s^{-2} and median LCLml 747 m/SD 310 m), or other nontrivial longevities from their 6300 grid-hour tornado events between 2009 and 2015}, and statements in *Storm Data* indicate this tornado was not continuous for 99.8 mi. Based on NCEI and *Storm Data,* a long-lived supercell produced five shorter-lived tornadoes with PLs, widths, and times noted above. The tornadoes were rated F1 by NCEI, noting that only the second tornado had reports of "mesquite trees uprooted and a few fences down" in Kinney County along a swath southwest and south of Spofford, Texas. The information in the SPC tornado database is 242, 1980, 05, 15, 1980–05–15, 1715:00, 3, TX, 48, 53, 1, 0, 0, 0.0, 0.0, 29.27, −100.78, 28.73, −99.28, 99.8, 40, 1, 1, 1, 465, 271, 323, 507, 0.
2) Also removed from the SPC dataset was a 3–4 April 1981 Iowa, F0, 50-yd-wide, 103.5-mi PL tornado report. In this case, the reported 103.5-mi PL was in conflict with the associated starting and ending latitude and longitude points, which represented a distance of 46.1 mi. Furthermore, consultation with the NCEI *Storm Data* publication showed a date discrepancy where NCEI dates were 4–5 April 1981 for the same counties and start time; however, the SPC 3–4 April 1981 dates were corroborated by a Quad-City Times newspaper article (5 April 1981; courtesy of Doris Grazulis). The NCEI *Storm Data* publication lists this tornado PL at ~50 mi and "mostly skipping." Examination of the tornado track segment paths in the NCEI "Bulk Data Download" (Fig. A1, top) shows an impossible (in the presence of strong mid- and upper-level southwesterly flow) track of four segments, including a 32-mi track directed southeast to northwest, that when all four segments are added together remarkably has a total of 103.5 mi. The change in track

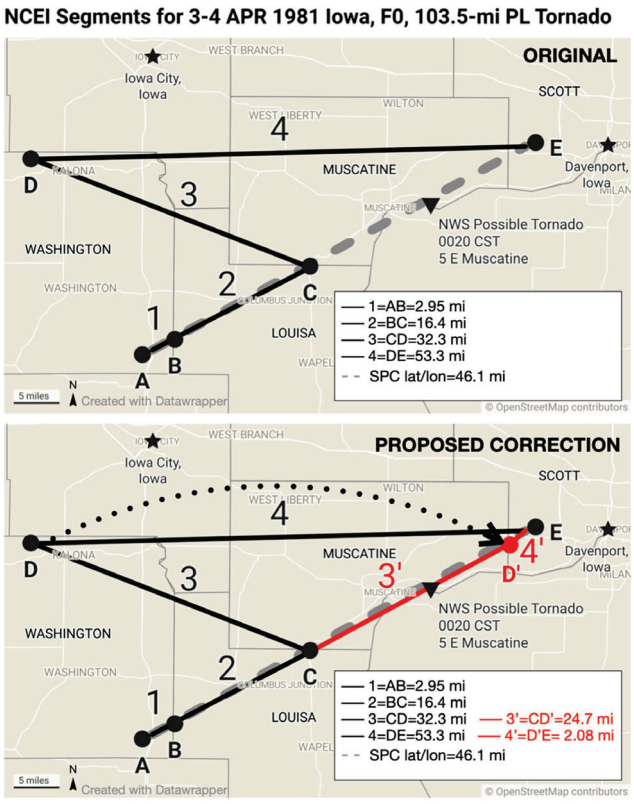

FIG. A1. (top) NCEI segment data of the track of a 3–4 Apr 1981 southeast Iowa tornado for four pathlength segment distances that add up to a total pathlength of 103.5 mi (black). (bottom) A proposed correction to the longitude of point D moves the intersection of the two segments (3 and 4) to location D′ (new segments 3′ and 4′ in red) and results in a new total pathlength of ~46 mi. The SPC latitude and longitude coordinates are from point A to point E for a calculated distance of 46.1 mi (thick gray dashed), despite SPC's reported PL of 103.5 mi. County names that contain the segments are shown in black capital letters. The location of a possible tornado reported by the NWS is denoted by an upside-down black triangle (Quad-City Times, 5 Apr 1981, courtesy of Doris Grazulis).

direction occurred at the Louisa–Muscatine county line, consistent with segment termination and start points that typically occur at county lines, but the segment 3–4 intersection point in Washington county is not at a county line and does account for the very unlikely total PL of 103.5 mi.

1) Further examination of the segment data showed that there was probably a typographical error in the longitude of the intersection point of segments 3 and 4 (Fig. A1, top, point D). The reported longitude for this intersection point (i.e., the ending longitude of segment 3 and the beginning longitude of segment 4) was −91.78°. If this value is replaced with −90.78° (see bold and italicized values in Table A1), the resulting intersection point (in Fig A1, bottom, move point D to point D′) would lie at the Muscatine–Scott county line (consistent with conventional segment termination points) and would be aligned with the SPC track (gray dashed, Fig. A1) plotted based on SPC's latitude and longitude (despite SPC's reported 103.5-mi PL). Consistently, the originating county for segment 4 is reported by NCEI to be Scott County (Table A1, bold and italicized) and not Washington County, and the resulting corrected total PL of the four segments would become ~46 mi (which is consistent with SPC's latitude-and-longitude-based calculated PL). Last, the proposed corrected track would also be consistent with the NWS's possible tornado report 5 mi east of Muscatine, Iowa, that was reported in the Quad-City Times newspaper article (5 April 1981).
2) Additionally, for the elapsed time of ~75 min (*Storm Data* publication), the storm speed would have to have been 82.8 mph for a PL = 103.5 mi. In contrast, an ERA sounding (not shown) at 41.50° latitude and −90.75° longitude at 0000 UTC 4 April 1981 provided a storm motion of 229° at 26.3 m s^{-1} or 58.8 mph. An NWS observed sounding at Peoria, Illinois (KPIA; not shown), 0000 UTC 4 April was comparable. The ≥80-mph storm speed is highly improbable given that midlevel environmental wind speeds did not exceed 80 mph until above ~5.5 km. Furthermore, both soundings show an equilibrium level of a rather shallow 8–9 km and weak CAPEml (CAPEmu) of 494 J kg^{-1} (634 J kg^{-1}) in the ERA5 sounding and 169 J kg^{-1} (425 J kg^{-1}) in the KPIA sounding.
3) Therefore, we propose that this tornado track is not a continuous 103.5-mi-long track, due to a likely typographical error that is readily corrected by changing the longitude of both the end of segment 3 and start of segment 4 from −91.78° to −90.78°. These corrections result in a 46.1-mi, skipping, F0, tornado track. The information in the SPC tornado database is as follows: 75, 1981, 04, 03, 1981-04-03, 23:15:00, 3, IA, 19, 5, 0, 0, 0, 5.0, 0.0, 41.2, −91.53, 41.52, −90.75, 103.5, 50, 1, 1, 1, 183, 115, 139, 163, 0.

TABLE A1. NCEI "Bulk Data Download" segment data for 3–4 Apr 1981, southeastern Iowa, F0, 103-mi PL tornado. Proposed correction to the end longitude of segment 3 and the start longitude in segment 4 bold and italicized. The proposed correction would be consistent with Scott County being reported for the fourth segment (bold and italicized).

Segment No.	Segment	County	Date in 1981	Time (UTC)	F scale	PL (mi)	Width (yards)	Start lat (°)	Start lon (°)	End lat (°)	End lon (°)
1	AB	Washington	3 Apr	0515	0	1.3	50	41.20	−91.53	41.22	−91.48
2	BC	Louisa	3 Apr	0518	0	16.6	33	41.22	−91.48	41.33	−91.20
3	CD	Muscatine	3 Apr	0555	0	32.2	33	41.33	−91.20	41.50	***Change −91.78 to −90.78***
4	DE	***Scott***	4 Apr	0630	0	53.4	33	41.50	***Change −91.78 to −90.78***	41.52	–90.75

APPENDIX B

Student's *t*-test Statistics *p* Values and Means

Table B1 shows Student's *t*-test statistics *p*-values for differences in the means of variables when comparing variables for various pathlength bins. Means for each variable for relevant pathlength bins are included. Student's *t*-test values are generally more significant (bolded numbers, ≤0.001) for kinematic variable comparisons, which tended have smaller skewness than thermodynamic variables.

TABLE B1. Student's *t*-test statistics *p* values for difference in means (e.g., first column of *p* values compares values for PL < 10 mi to values for PL ≥ 10 mi) for ERA5 vertical profile parameters as a function of pathlength bins that were considered. Bold numbers are *p* values ≤ 0.001 (all <0.001 listed as ≤0.001), and normal text are *p* values > 0.001. The population means are in the eight columns on the right. Numbers of cases used in each pathlength bin (units of mi) are included at the top of the table with the mean value headers. See the supplemental material for a complete list of parameter results.

Student's *t*-test *p* values and mean	*p* value									Mean							
	<10 ≥10	<10 ≥30	<10 30–60	<10 30–90	<10 60–90	<10 ≥90	<30 ≥30	30–60 ≥90	30–90 ≥90	<10 41 801	≥10 3775	<30 45 120	≥30 456	30–60 385	30–90 442	60–90 57	≥90 14
CAPEml	0.797	0.044	0.190	0.068	0.088	0.224	0.043	0.294	0.338	900.87	904.45	900.42	974.46	952.78	968.81	1077.04	1152.83
CAPE03ml	**0.001**	**0.001**	**0.001**	**0.001**	0.042	0.901	**0.001**	0.596	0.563	58.01	61.87	58.26	65.79	65.56	65.99	68.92	59.43
CINml	0.858	0.199	0.377	0.275	0.454	0.012	0.195	0.034	0.037	45.11	44.94	45.13	41.86	42.67	42.29	39.75	28.04
LCLml	**0.001**	**0.001**	**0.001**	**0.001**	0.004	0.003	**0.001**	0.501	0.505	959.06	816.42	949.08	765.47	769.22	767.39	754.97	704.85
CAPEmu	0.078	0.080	0.250	0.111	0.151	0.268	0.067	0.301	0.343	1316.33	1288.97	1313.27	1392.38	1370.38	1386.18	1492.90	1588.33
WSSFC	**0.001**	**0.001**	**0.001**	**0.001**	0.401	0.017	**0.001**	0.098	0.080	4.21	4.67	4.24	4.74	4.75	4.71	4.45	5.62
WS500	**0.001**	**0.001**	**0.001**	**0.001**	**0.001**	**0.001**	**0.001**	**0.001**	**0.001**	12.47	15.86	12.71	17.00	16.91	16.87	16.66	21.11
WS1000	**0.001**	**0.001**	**0.001**	**0.001**	**0.001**	**0.001**	**0.001**	0.003	0.002	15.04	19.877	15.38	21.40	21.19	21.24	21.61	26.43
WS4000	**0.001**	**0.001**	**0.001**	**0.001**	**0.001**	**0.001**	**0.001**	**0.001**	0.002	20.64	26.62	21.05	28.89	28.50	28.72	30.18	34.16
WS6000	**0.001**	**0.001**	**0.001**	**0.001**	**0.001**	**0.001**	**0.001**	0.098	0.119	23.70	30.09	24.14	32.49	32.20	32.40	33.72	35.41
WS9000	**0.001**	**0.001**	**0.001**	**0.001**	**0.001**	**0.001**	**0.001**	0.188	0.242	27.58	34.07	28.03	36.66	36.19	36.57	39.10	39.44
WSLLmax	**0.001**	**0.001**	**0.001**	**0.001**	**0.001**	**0.001**	**0.001**	0.015	0.013	17.76	22.94	18.12	24.55	24.38	24.42	24.74	28.69
WSULmax	**0.001**	**0.001**	**0.001**	**0.001**	**0.001**	**0.001**	**0.001**	0.186	0.242	29.18	35.69	29.63	38.12	37.66	38.04	40.63	40.76
SRWSSFC	**0.001**	**0.001**	**0.001**	**0.001**	**0.001**	**0.001**	**0.001**	0.035	0.042	15.04	18.73	15.29	20.33	20.10	20.25	21.24	22.80
SRWS6000	**0.001**	**0.001**	**0.001**	**0.001**	0.189	0.210	**0.001**	0.053	0.053	10.76	11.26	10.80	11.33	11.39	11.39	11.37	9.58
BWD500	**0.001**	**0.001**	**0.001**	**0.001**	**0.001**	**0.001**	**0.001**	0.003	0.002	8.65	11.47	8.85	12.48	12.37	12.39	12.50	15.58
BWD1000	**0.001**	**0.001**	**0.001**	**0.001**	**0.001**	**0.001**	**0.001**	0.009	0.008	11.90	15.97	12.19	17.31	17.09	17.18	17.81	21.14
BWD4000	**0.001**	**0.001**	**0.001**	**0.001**	**0.001**	**0.001**	**0.001**	0.010	0.014	19.12	24.02	19.46	25.88	25.55	25.76	27.21	29.59
BWD6000	**0.001**	**0.001**	**0.001**	**0.001**	**0.001**	**0.001**	**0.001**	0.300	0.351	22.41	27.77	22.79	29.72	29.48	29.67	30.96	31.33
BWD9000	**0.001**	**0.001**	**0.001**	**0.001**	**0.001**	**0.001**	**0.001**	0.397	0.488	26.45	32.01	26.83	34.18	33.76	34.13	36.60	35.75
BWDLLmax	**0.001**	**0.001**	**0.001**	**0.001**	**0.001**	**0.001**	**0.001**	0.075	0.075	15.25	19.65	15.56	20.99	20.83	20.91	21.39	23.70
BWDULmax	**0.001**	**0.001**	**0.001**	**0.001**	**0.001**	**0.001**	**0.001**	0.408	0.507	27.98	33.57	28.37	35.63	35.21	35.59	38.11	37.06
SRH500	**0.001**	**0.001**	**0.001**	**0.001**	**0.001**	**0.001**	**0.001**	0.187	0.183	117.85	183.95	122.47	207.18	205.60	206.09	209.39	241.52
SRH1000	**0.001**	**0.001**	**0.001**	**0.001**	**0.001**	**0.001**	**0.001**	0.231	0.229	171.30	256.38	177.30	281.81	279.64	280.51	286.38	322.82
SRH3000	**0.001**	**0.001**	**0.001**	**0.001**	**0.001**	0.002	**0.001**	0.487	0.481	244.10	335.34	250.59	356.53	355.36	355.63	357.46	384.83
SRMLIKE500	**0.001**	**0.001**	**0.001**	**0.001**	**0.001**	0.016	**0.001**	0.907	0.864	232.22	300.02	236.97	323.18	321.32	323.37	337.25	317.12
CA500	**0.001**	**0.001**	**0.001**	**0.001**	**0.001**	**0.001**	**0.001**	0.030	0.033	73.12	58.10	72.07	52.81	53.85	53.19	48.69	41.01
STPcin500	**0.001**	**0.001**	**0.001**	**0.001**	**0.001**	**0.001**	**0.001**	0.021	0.029	0.98	1.75	1.03	2.39	2.29	2.35	2.71	3.70
VTPcin500	**0.001**	**0.001**	**0.001**	**0.001**	**0.001**	**0.001**	**0.001**	0.395	0.461	1.56	2.89	1.65	3.98	3.80	3.94	4.90	5.02
EHI500	**0.001**	**0.001**	**0.001**	**0.001**	**0.001**	**0.001**	**0.001**	0.055	0.068	0.57	0.95	0.59	1.26	1.22	1.24	1.40	1.79
Bunkers time	**0.001**	**0.001**	**0.001**	**0.001**	**0.001**	**0.001**	**0.001**	**0.001**	**0.001**	3.21	26.98	4.66	56.52	49.89	54.10	82.49	132.99
V_{Bunkers}	**0.001**	**0.001**	**0.001**	**0.001**	**0.001**	**0.001**	**0.001**	0.006	0.006	15.75	20.56	16.08	22.59	22.31	22.47	23.55	26.65
LTTP	**0.001**	**0.001**	**0.001**	**0.001**	**0.001**	0.006	**0.001**	0.019	0.037	29.98	96.66	34.11	173.42	160.71	169.06	225.46	311.25
LTTPt	**0.001**	**0.001**	**0.001**	**0.001**	**0.001**	0.002	**0.001**	0.051	0.077	1.72	1.93	1.73	2.21	2.15	2.19	2.48	2.88
LTTPk	**0.001**	**0.001**	**0.001**	**0.001**	**0.001**	**0.001**	**0.001**	0.137	0.157	742.62	1825.72	815.67	2480.95	2394.79	2449.07	2815.70	3487.58

APPENDIX C

Cohen's *d*-values and Standard Deviations

Table C1 shows Student's *t*-test Cohen's *d* values to indicate effect size of the Student's *t*-test *p* values when comparing variables for various pathlength bins. Standard deviations (SD) for pathlength bins are included. Effect size generally was medium (≥0.5) to large for most kinematic variables, but not thermodynamic variables, which tended to be skewed.

TABLE C1. Cohen's *d* values with Student's *t*-test statistics for ERA5 vertical profile parameters as a function of pathlength bins. Bold, italicized numbers are *d* values ≥ 0.8, bold numbers are *d* values ≥ 0.5–0.8, and normal text are *d* values <0.5. Cohen *d* values of 0.2–0.5, 0.5–0.8, and ≥0.8 indicate small, medium, and large effect size, respectively, and can be interpreted as the number of standard deviations between two means. The standard deviations (SD) are in the eight columns on the right side of the table. Numbers of cases in each pathlength bin (units of mi) are with the standard deviation headers. See the supplemental material for a complete list of parameter results.

Cohen *d* values and standard deviations (SD)	*d* value									SD							
	<10 ≥10	<10 ≥30	<10 30–60	<10 30–90	<10 60–90	<10 ≥90	<30 ≥30	30–60 ≥90	30–90 ≥90	<10 41 801	≥10 3775	<30 45 120	≥30 456	30–60 385	30–90 442	60–90 57	≥90 14
CAPEml	0.00	0.10	0.07	0.09	0.23	0.33	0.10	0.29	0.26	770.77	736.75	768.62	701.79	697.25	702.63	735.15	674.79
CAPE03ml	0.10	0.19	0.19	0.20	0.27	0.04	0.19	0.15	0.16	39.96	40.54	40.00	40.84	41.58	41.18	38.61	28.44
CINml	0.00	0.06	0.05	0.05	0.10	0.32	0.06	0.33	0.32	53.82	50.14	53.60	45.03	45.34	45.52	47.02	21.68
LCLml	0.28	0.37	0.37	0.37	0.39	0.49	0.36	0.18	0.18	518.03	386.26	511.01	343.72	353.20	346.23	297.25	253.88
CAPEmu	0.03	0.08	0.06	0.08	0.19	0.30	0.09	0.28	0.26	911.44	831.44	906.27	778.38	770.15	777.90	827.60	796.97
WSSFC	0.21	0.24	0.24	0.23	0.11	**0.64**	0.22	0.45	0.48	2.20	2.21	2.21	1.88	1.93	1.89	1.51	1.55
WS500	**0.55**	**0.74**	**0.72**	**0.72**	**0.68**	***1.40***	**0.69**	***0.89***	***0.91***	6.16	5.67	6.19	4.69	4.79	4.69	3.95	2.46
WS1000	**0.63**	***0.83***	***0.80***	***0.80***	***0.85***	***1.48***	**0.78**	***0.84***	***0.86***	7.72	7.04	7.77	6.12	6.29	6.11	4.68	4.01
WS4000	**0.74**	***1.02***	***0.97***	***1.00***	***1.18***	***1.67***	***0.96***	***0.90***	***0.88***	8.11	7.24	8.19	6.27	6.32	6.24	5.47	4.89
WS6000	**0.72**	***0.98***	***0.95***	***0.97***	***1.11***	***1.30***	***0.92***	0.45	0.43	9.00	8.07	9.08	7.02	7.13	7.06	6.50	5.13
WS9000	**0.58**	***0.81***	***0.77***	***0.80***	***1.03***	***1.06***	**0.76**	0.36	0.32	11.24	10.30	11.29	8.94	9.07	9.03	8.39	4.98
WSLLmax	**0.67**	***0.87***	***0.85***	***0.85***	***0.89***	***1.40***	***0.82***	**0.68**	**0.69**	7.82	7.08	7.88	6.23	6.42	6.25	4.97	4.11
WSULmax	**0.61**	***0.84***	***0.80***	***0.83***	***1.07***	***1.09***	**0.79**	0.36	0.32	10.67	9.71	10.74	8.46	8.60	8.53	7.62	5.31
SRWSSFC	**0.68**	***0.97***	***0.93***	***0.95***	***1.13***	***1.42***	***0.91***	**0.59**	**0.56**	5.48	5.18	5.54	4.54	4.61	4.54	3.92	4.08
SRWS6000	0.14	0.16	0.18	0.18	0.18	0.34	0.15	**0.53**	**0.53**	3.51	3.54	3.52	3.42	3.41	3.42	3.48	3.07
BWD500	**0.59**	***0.80***	**0.78**	**0.78**	***0.80***	***1.44***	**0.76**	***0.84***	***0.85***	4.81	4.32	4.83	3.78	3.87	3.78	3.11	2.30
BWD1000	**0.63**	***0.83***	***0.80***	***0.82***	***0.91***	***1.42***	**0.79**	**0.74**	**0.74**	6.49	5.87	6.53	5.39	5.53	5.39	4.26	3.94
BWD4000	**0.69**	***0.95***	***0.90***	***0.93***	***1.13***	***1.47***	***0.89***	**0.71**	**0.68**	7.14	6.35	7.19	5.68	5.71	5.66	5.12	5.28
BWD6000	**0.67**	***0.90***	***0.87***	***0.90***	***1.05***	***1.10***	***0.85***	0.28	0.26	8.11	7.23	8.16	6.51	6.59	6.55	6.17	5.05
BWD9000	**0.53**	**0.73**	**0.69**	**0.72**	***0.96***	***0.88***	**0.69**	0.23	0.19	10.62	9.69	10.65	8.61	8.72	8.69	8.17	5.00
BWDLLmax	**0.65**	***0.84***	***0.82***	***0.83***	***0.90***	***1.24***	**0.79**	0.49	0.49	6.83	6.13	6.87	5.68	5.83	5.70	4.69	4.30
BWDULmax	**0.56**	**0.76**	**0.72**	**0.76**	***1.01***	***0.90***	**0.72**	0.23	0.18	10.04	9.08	10.08	8.12	8.24	8.19	7.47	5.13
SRH500	**0.64**	***0.86***	***0.85***	***0.85***	***0.88***	***1.19***	***0.81***	0.36	0.37	103.63	104.93	105.07	96.95	99.57	97.37	81.62	77.65
SRH1000	**0.61**	**0.79**	**0.78**	**0.78**	***0.83***	***1.09***	**0.74**	0.33	0.33	139.25	139.49	140.97	128.26	131.75	128.77	107.25	106.89
SRH3000	**0.54**	**0.66**	**0.66**	**0.66**	**0.67**	***0.83***	**0.62**	0.19	0.19	169.37	168.81	171.04	151.71	155.92	152.50	128.14	125.47
SRMLIKE500	**0.52**	**0.70**	**0.68**	**0.70**	***0.81***	**0.65**	**0.66**	0.03	0.05	130.30	131.25	131.50	124.57	123.54	125.38	137.53	98.97
CA500	0.40	**0.53**	**0.51**	**0.52**	**0.64**	***0.84***	**0.51**	**0.61**	**0.59**	38.14	25.89	37.59	20.59	21.50	20.72	13.71	11.02
STPcin500	**0.56**	***1.06***	***0.99***	***1.03***	***1.31***	***2.06***	***0.99***	**0.64**	**0.61**	1.32	1.83	1.37	2.24	2.20	2.22	2.40	2.53
VTPcin500	0.44	***0.82***	**0.76**	***0.81***	***1.15***	***1.19***	**0.76**	0.23	0.20	2.90	4.38	3.03	5.37	5.30	5.41	6.06	4.20
EHI500	**0.52**	***0.96***	***0.90***	***0.93***	***1.15***	***1.71***	***0.90***	**0.53**	**0.51**	0.72	0.92	0.74	1.09	1.08	1.08	1.14	1.19
Bunkers time	***3.53***	***10.06***	***9.47***	***10.01***	***16.83***	***27.61***	***6.60***	***4.78***	***3.88***	4.68	17.51	7.50	24.45	16.94	20.08	16.28	27.53
V_{Bunkers}	**0.70**	***0.99***	***0.95***	***0.97***	***1.13***	***1.58***	***0.93***	**0.79**	**0.78**	6.92	6.42	6.99	5.44	5.55	5.43	4.42	4.05
LTTP	**0.66**	***1.52***	***1.40***	***1.48***	***2.13***	***3.08***	***1.38***	**0.65**	**0.58**	91.11	171.99	98.50	245.69	229.38	242.81	315.87	302.62
LTTPt	0.15	0.35	0.31	0.34	**0.55**	***0.84***	0.34	**0.54**	0.49	1.39	1.39	1.39	1.41	1.37	1.41	1.64	1.28
LTTPk	**0.61**	***1.02***	***0.97***	***1.48***	***1.22***	***1.62***	***0.93***	0.41	0.39	1698.02	2470.53	1781.32	2651.02	2638.37	2643.27	2670.60	2799.06

APPENDIX D

Mann–Whitney *U* Statistic *p* Values

Table D1 shows Mann–Whitney *U* (MWU) statistic *p* values when comparing variables for various pathlength bins. The MWU *p* values were significant (<0.001) for most variables except some thermodynamics variables and most variables for longest intra-pathlength comparisons.

TABLE D1. Mann–Whitney U (MWU) statistic p values for ERA5 vertical profile parameters as a function of pathlength bins. Bold numbers are p values ≤ 0.001 (all values < 0.001 listed as ≤0.001), and normal text are p values > 0.001. Pathlength bins are in miles. See the supplemental material for a more complete list of parameter results.

	p value								
MWU p value	<10 ≥10	<10 ≥30	<10 30–60	<10 30–90	<10 60–90	<10 ≥90	<30 ≥30	30–60 ≥90	30–90 ≥90
PL	**0.001**	**0.001**	**0.001**	**0.001**	**0.001**	**0.001**	**0.001**	**0.001**	**0.001**
E(F) scale	**0.001**	**0.001**	**0.001**	**0.001**	**0.001**	**0.001**	**0.001**	**0.001**	**0.001**
CAPEml	0.014	**0.001**	0.002	**0.001**	0.013	0.042	**0.001**	0.070	0.090
CAPE03ml	**0.001**	**0.001**	**0.001**	**0.001**	0.008	0.270	**0.001**	0.411	0.383
CINml	0.002	0.398	0.286	0.353	0.339	0.258	0.431	0.229	0.245
LCLml	**0.001**	**0.001**	**0.001**	**0.001**	**0.001**	0.021	**0.001**	0.312	0.313
CAPEmu	0.406	**0.001**	0.003	**0.001**	0.023	0.057	**0.001**	0.061	0.075
WSSFC	**0.001**	**0.001**	**0.001**	**0.001**	0.036	**0.001**	**0.001**	0.032	0.025
WS500	**0.001**	**0.001**	**0.001**	**0.001**	**0.001**	**0.001**	**0.001**	**0.001**	**0.001**
WS1000	**0.001**	**0.001**	**0.001**	**0.001**	**0.001**	**0.001**	**0.001**	**0.001**	**0.001**
WS4000	**0.001**	**0.001**	**0.001**	**0.001**	**0.001**	**0.001**	**0.001**	**0.001**	**0.001**
WS6000	**0.001**	**0.001**	**0.001**	**0.001**	**0.001**	**0.001**	**0.001**	0.051	0.061
WS9000	**0.001**	**0.001**	**0.001**	**0.001**	**0.001**	**0.001**	**0.001**	0.069	0.099
WSLLmax	**0.001**	**0.001**	**0.001**	**0.001**	**0.001**	**0.001**	**0.001**	0.004	0.003
WSULmax	**0.001**	**0.001**	**0.001**	**0.001**	**0.001**	**0.001**	**0.001**	0.075	0.104
SRWSSFC	**0.001**	**0.001**	**0.001**	**0.001**	**0.001**	**0.001**	**0.001**	0.018	0.022
SRWS6000	**0.001**	**0.001**	**0.001**	**0.001**	0.051	0.184	**0.001**	0.040	0.040
BWD500	**0.001**	**0.001**	**0.001**	**0.001**	**0.001**	**0.001**	**0.001**	**0.001**	**0.001**
BWD1000	**0.001**	**0.001**	**0.001**	**0.001**	**0.001**	**0.001**	**0.001**	0.003	0.003
BWD4000	**0.001**	**0.001**	**0.001**	**0.001**	**0.001**	**0.001**	**0.001**	0.007	0.010
BWD6000	**0.001**	**0.001**	**0.001**	**0.001**	**0.001**	**0.001**	**0.001**	0.188	0.214
BWD9000	**0.001**	**0.001**	**0.001**	**0.001**	**0.001**	**0.001**	**0.001**	0.194	0.241
BWDLLmax	**0.001**	**0.001**	**0.001**	**0.001**	**0.001**	**0.001**	**0.001**	0.022	0.023
BWDULmax	**0.001**	**0.001**	**0.001**	**0.001**	**0.001**	**0.001**	**0.001**	0.182	0.237
SRH500	**0.001**	**0.001**	**0.001**	**0.001**	**0.001**	**0.001**	**0.001**	0.095	0.099
SRH1000	**0.001**	**0.001**	**0.001**	**0.001**	**0.001**	**0.001**	**0.001**	0.116	0.116
SRH3000	**0.001**	**0.001**	**0.001**	**0.001**	**0.001**	**0.001**	**0.001**	0.177	0.175
SRMLIKE500	**0.001**	**0.001**	**0.001**	**0.001**	**0.001**	**0.001**	**0.001**	0.476	0.447
CA500	**0.001**	**0.001**	**0.001**	**0.001**	**0.001**	**0.001**	**0.001**	0.003	0.004
STPcin500	**0.001**	**0.001**	**0.000**	**0.001**	**0.001**	**0.001**	**0.001**	0.007	0.009
VTPcin500	**0.001**	**0.001**	**0.000**	**0.001**	**0.001**	**0.001**	**0.001**	0.030	0.038
EHI500	**0.001**	**0.001**	**0.001**	**0.001**	**0.001**	**0.001**	**0.001**	0.018	0.022
Bunkers time	**0.001**	**0.001**	**0.001**	**0.001**	**0.001**	**0.001**	**0.001**	**0.001**	**0.001**
V_{Bunkers}	**0.001**	**0.001**	**0.001**	**0.001**	**0.001**	**0.001**	**0.001**	0.002	0.002
LTTP	**0.001**	**0.001**	**0.001**	**0.001**	**0.001**	**0.001**	**0.001**	0.005	0.006
LTTPt	**0.001**	**0.001**	**0.001**	**0.001**	**0.001**	**0.001**	**0.001**	0.021	0.032
LTTPk	**0.001**	**0.001**	**0.001**	**0.001**	**0.001**	**0.001**	**0.001**	0.020	0.024

APPENDIX E

Mann–Whitney U f Values

Table E1 shows Mann–Whitney U (MWU) f values to indicate effect size of MWU p values when comparing variables for various pathlength bins. Bold, italicized numbers are ≥0.8 indicating large effect size, bold numbers are 0.65–0.8 indicating medium effect size, and <0.65 are regular text indicating small effect size. Effect size was mostly small for thermodynamic variables and medium to large for most kinematic variables.

TABLE E1. Mann–Whitney U (MWU) statistic f values [f = U1/($n_1 \times n_2$), where U1 is the MWU U value of the shorter PL bin. Bold, italicized numbers are f values ≥ 0.80, bold numbers are f values 0.65–0.8, while regular text are f values < 0.65, where f values = <0.65, 0.65–0.8, and ≥0.8 could be considered small, medium, and large effect size, respectively. Pathlength bins are in miles. See the supplemental material for a more complete list of parameter results.

	f								
MWU f, f = U1/($n_1 \times n_2$)	<10 ≥10	<10 ≥30	<10 30–60	<10 30–90	<10 60–90	<10 ≥90	<30 ≥30	30–60 ≥90	30–90 ≥90
PL	***1.000***	***1.000***	***1.000***	***1.000***	***1.000***	***1.000***	***1.000***	***1.000***	***1.000***
E(F) scale	***0.833***	***0.935***	***0.925***	***0.933***	***0.987***	***0.998***	***0.922***	***0.847***	***0.834***
CAPEml	0.511	0.552	0.544	0.549	0.585	0.634	0.551	0.616	0.605
CAPE03ml	0.530	0.559	0.555	0.560	0.593	0.547	0.557	0.482	0.477
CINml	0.514	0.504	0.508	0.505	0.484	0.450	0.502	0.442	0.446
LCLml	0.415	0.378	0.379	0.379	0.383	0.343	0.384	0.461	0.462
CAPEmu	0.501	0.548	0.541	0.546	0.576	0.622	0.549	0.621	0.613
WSSFC	0.566	0.593	0.592	0.589	0.569	**0.730**	0.589	0.646	**0.654**
WS500	**0.662**	**0.722**	**0.718**	**0.717**	**0.712**	***0.897***	**0.711**	**0.779**	**0.784**
WS1000	**0.680**	**0.740**	**0.732**	**0.735**	**0.759**	***0.895***	**0.728**	**0.746**	**0.751**
WS4000	**0.711**	**0.791**	**0.780**	**0.787**	***0.835***	***0.921***	**0.778**	**0.752**	**0.745**
WS6000	**0.705**	**0.782**	**0.774**	**0.780**	***0.816***	***0.867***	**0.770**	0.629	0.622
WS9000	**0.672**	**0.747**	**0.736**	**0.745**	***0.802***	***0.836***	**0.736**	0.617	0.601
WSLLmax	**0.693**	**0.754**	**0.746**	**0.750**	**0.774**	***0.885***	**0.741**	**0.709**	**0.712**
WSULmax	**0.682**	**0.755**	**0.743**	**0.752**	***0.813***	***0.838***	**0.743**	0.613	0.599
SRWSSFC	**0.693**	**0.773**	**0.763**	**0.770**	***0.820***	***0.868***	**0.761**	**0.664**	**0.657**
SRWS6000	0.544	0.557	0.560	0.561	0.563	0.431	0.554	0.363	0.362
BWD500	**0.670**	**0.733**	**0.726**	**0.727**	**0.738**	***0.900***	**0.721**	**0.777**	**0.781**
BWD1000	**0.680**	**0.737**	**0.727**	**0.733**	**0.769**	***0.879***	**0.725**	**0.715**	**0.714**
BWD4000	**0.697**	**0.772**	**0.761**	**0.769**	***0.822***	***0.880***	**0.760**	**0.692**	**0.683**
BWD6000	**0.691**	**0.761**	**0.754**	**0.759**	**0.799**	***0.823***	**0.749**	0.570	0.562
BWD9000	**0.658**	**0.726**	**0.715**	**0.724**	**0.786**	**0.795**	**0.716**	0.568	0.555
BWDLLmax	**0.688**	**0.743**	**0.735**	**0.739**	**0.771**	***0.849***	**0.730**	**0.658**	**0.657**
BWDULmax	**0.667**	**0.735**	**0.723**	**0.733**	**0.798**	**0.798**	**0.724**	0.571	0.556
SRH500	**0.684**	**0.747**	**0.740**	**0.744**	**0.767**	***0.834***	**0.734**	0.603	0.601
SRH1000	**0.678**	**0.732**	**0.726**	**0.730**	**0.757**	***0.814***	**0.720**	0.594	0.594
SRH3000	**0.668**	**0.713**	**0.708**	**0.711**	**0.733**	**0.772**	**0.702**	0.573	0.573
SRMLIKE500	**0.660**	**0.715**	**0.711**	**0.715**	**0.739**	**0.730**	**0.704**	0.495	0.489
CA500	0.385	0.335	0.346	0.339	0.289	0.203	0.342	0.285	0.291
STPcin500	**0.658**	**0.732**	**0.723**	**0.728**	**0.764**	***0.858***	**0.725**	**0.693**	**0.685**
VTPcin500	0.627	**0.687**	**0.676**	**0.683**	**0.732**	***0.818***	**0.679**	0.648	0.639
EHI500	**0.654**	**0.732**	**0.723**	**0.729**	**0.767**	***0.828***	**0.723**	**0.665**	**0.658**
Bunkers time	***0.983***	***0.999***	***0.999***	***0.999***	***1.000***	***1.000***	***0.995***	***0.994***	***0.989***
V_{Bunkers}	**0.700**	**0.782**	**0.772**	**0.779**	***0.826***	***0.904***	**0.770**	**0.726**	**0.721**
LTTP	**0.709**	**0.794**	**0.781**	**0.789**	***0.844***	***0.930***	**0.782**	**0.703**	**0.695**
LTTPt	0.548	0.604	0.595	0.600	0.637	**0.733**	0.601	**0.660**	0.646
LTTPk	**0.710**	**0.785**	**0.774**	**0.782**	***0.834***	***0.894***	**0.772**	**0.662**	**0.655**

APPENDIX F

Mann–Whitney *U* Statistic Rank-Biserial Correlation *r* Values

Table F1 shows Mann–Whitney U (MWU) statistic rank-biserial correlation r values to indicate effect size of MWU p values when comparing variables for various pathlength bins. Bold, italicized numbers are $|r$ values$|$ ≥ 0.5, bold numbers are $|r$ values$|$ ≥ 0.3–0.5, and regular text are $|r$ values$|$ < 0.3. Effect size was most small for thermodynamic variables and large for most kinematic variables.

TABLE F1. Mann–Whitney U (MWU) statistic rank-biserial correlation r values [$r = 2U1/(n_1 \times n_2) - 1 = 1 - 2U2/(n_1 \times n_2)$], where, in this paper, U1 is the MWU U value for the shorter PL bin ($f = U1/(n_1 \times n_2)$ in appendix E) and U2 is the MWU U value for the longer PL bin. Bold, italicized numbers are $|r$ values$| \geq 0.5$, bold numbers are $|r$ values$| \geq 0.3$–0.5, and regular text are $|r$ values$| < 0.3$. Values of $|r| = 0.1$–0.3, 0.3–0.5, ≥ 0.5 could indicate small, medium, and large effect size. Negative numbers are inversely related. Pathlength bins are in miles. See the supplemental material for a more complete list of parameter results.

MWU r, $r = 2\ U1/(n_1 \times n_2) - 1 = 1 - 2U2/(n_1 \times n_2)$	r								
	<10 ≥10	<10 ≥30	<10 30–60	<10 30–90	<10 60–90	<10 ≥90	<30 ≥30	30–60 ≥90	30–90 ≥90
PL	***1.000***	***1.000***	***1.000***	***1.000***	***1.000***	***1.000***	***1.000***	***1.000***	***1.000***
E(F) scale	***0.665***	***0.871***	***0.851***	***0.867***	***0.974***	***0.996***	***0.843***	***0.694***	***0.669***
CAPEml	0.022	0.103	0.087	0.098	0.170	0.267	0.103	0.232	0.211
CAPE03ml	0.060	0.118	0.109	0.119	0.186	0.095	0.115	−0.035	−0.047
CINml	0.028	0.007	0.017	0.010	−0.032	−0.100	0.005	−0.117	−0.108
LCLml	−0.170	−0.244	−0.243	−0.242	−0.234	**−0.314**	-0.232	−0.077	−0.076
CAPEmu	0.002	0.096	0.082	0.091	0.153	0.244	0.097	0.243	0.226
WSSFC	0.132	0.187	0.184	0.178	0.138	**0.461**	0.177	0.292	**0.307**
WS500	**0.323**	**0.445**	**0.435**	**0.434**	**0.424**	***0.795***	**0.422**	***0.558***	***0.568***
WS1000	**0.361**	**0.481**	**0.464**	**0.471**	***0.518***	***0.789***	**0.456**	**0.493**	***0.503***
WS4000	**0.423**	***0.582***	***0.560***	***0.574***	***0.669***	***0.841***	***0.556***	***0.503***	**0.491**
WS6000	**0.409**	***0.564***	***0.548***	***0.559***	***0.632***	***0.735***	***0.540***	0.257	0.243
WS9000	**0.345**	**0.495**	**0.472**	**0.489**	***0.604***	***0.672***	**0.473**	0.233	0.202
WSLLmax	**0.387**	***0.508***	**0.492**	***0.500***	***0.548***	***0.769***	**0.482**	**0.417**	**0.424**
WSULmax	**0.363**	***0.510***	**0.486**	***0.504***	***0.626***	***0.675***	**0.487**	0.227	0.197
SRWSSFC	**0.386**	***0.547***	***0.526***	***0.541***	***0.640***	***0.735***	***0.522***	**0.328**	**0.315**
SRWS6000	0.088	0.113	0.120	0.121	0.125	−0.139	0.107	−0.275	−0.275
BWD500	**0.341**	**0.465**	**0.451**	**0.454**	**0.477**	***0.800***	**0.442**	***0.554***	***0.561***
BWD1000	**0.360**	**0.474**	**0.455**	**0.465**	***0.539***	***0.758***	**0.451**	**0.429**	**0.429**
BWD4000	**0.394**	***0.544***	***0.522***	***0.537***	***0.645***	***0.760***	***0.520***	**0.384**	**0.367**
BWD6000	**0.381**	***0.523***	***0.507***	***0.519***	***0.598***	***0.646***	**0.499**	0.140	0.124
BWD9000	**0.316**	**0.452**	**0.430**	**0.448**	***0.572***	***0.591***	**0.432**	0.136	0.111
BWDLLmax	**0.375**	**0.486**	**0.470**	**0.479**	***0.542***	***0.698***	**0.461**	**0.316**	**0.314**
BWDULmax	**0.335**	**0.469**	**0.446**	**0.465**	***0.595***	***0.597***	**0.448**	0.142	0.112
SRH500	**0.367**	**0.493**	**0.481**	**0.488**	***0.533***	***0.669***	**0.469**	0.206	0.202
SRH1000	**0.357**	**0.465**	**0.451**	**0.459**	***0.515***	***0.629***	**0.440**	0.188	0.187
SRH3000	**0.335**	**0.427**	**0.417**	**0.423**	**0.466**	***0.545***	**0.403**	0.146	0.147
SRMLIKE500	**0.321**	**0.430**	**0.422**	**0.429**	**0.478**	**0.460**	**0.408**	−0.010	−0.021
CA500	−0.231	**−0.331**	**−0.308**	**−0.322**	**−0.423**	***−0.593***	**−0.316**	**−0.430**	**−0.419**
STPcin500	**0.315**	**0.464**	**0.446**	**0.456**	***0.527***	***0.715***	**0.446**	**0.387**	**0.369**
VTPcin500	0.254	**0.374**	**0.352**	**0.366**	**0.463**	***0.637***	**0.321**	0.297	0.279
EHI500	**0.308**	**0.463**	**0.446**	**0.457**	***0.535***	***0.655***	**0.445**	**0.329**	**0.315**
Bunkers time	***0.967***	***0.998***	***0.997***	***0.998***	***1.000***	***1.000***	***0.990***	***0.988***	***0.978***
$V_{Bunkers}$	**0.399**	***0.565***	***0.543***	***0.557***	***0.651***	***0.808***	***0.540***	**0.451**	**0.442**
LTTP	**0.419**	***0.587***	***0.563***	***0.579***	***0.688***	***0.860***	***0.563***	**0.405**	**0.390**
LTTPt	0.096	0.208	0.189	0.200	0.274	**0.466**	0.203	**0.320**	0.291
LTTPk	**0.420**	***0.571***	***0.548***	***0.564***	***0.668***	***0.788***	***0.545***	**0.323**	**0.310**

APPENDIX G

Maximum True Skill Scores and Optimum Values

Table G1 shows maximum true skill scores (TSSmax) and optimum values (Opt.) at TSSmax as a function of pathlength bins that were considered. Bold, italicized numbers are $|$TSSmax$| \geq 0.600$, bold numbers are $|$TSSmax$| \geq 0.400$, and normal text are $|$TSSmax$| < 0.400$. Values of $|$TSSmax$| = 0.2$–0.6, 0.6–0.8, and >0.8 are associated with forecasts with low, medium, and high skill. The best TSSmax were for kinematic variables when comparing the shorter pathlength bins with longer pathlength bins.

TABLE G1. Maximum true skill scores (TSS_{max}) and optimum values (Opt.) at TSS_{max} as a function of pathlength bins that were considered. Bold, italicized numbers are $|TSS_{max}| \geq 0.600$, bold black numbers are $|TSS_{max}| \geq 0.400$, and normal text are $|TSS_{max}| < 0.400$. Values of $|TSS_{max}| = 0.2$–0.6, 0.6–0.8, and >0.8 are associated with forecasts with low, medium, and high skill. Numbers of cases used in each pathlength bin (units of mi) are included at the top of the table in appendix C. The TSS_{max} values were determined from TSS values from 1000 values of a parameter from equally spaced intervals from 0 to Q3 + 1.5 IQR of any 10-mi PL subcategory or E(F)-scale category in the data. See the supplemental material for a more complete list of parameter results.

TSS_{max}, optimal value at TSS_{max}	TSS_{max}									Opt.								
	<10 ≥10	<10 ≥30	<10 30–60	<10 30–90	<10 60–90	<10 ≥90	<30 ≥30	30–60 ≥90	30–90 ≥90	<10 ≥10	<10 ≥30	<10 30–60	<10 30–90	<10 60–90	<10 ≥90	<30 ≥30	30–60 ≥90	30–90 ≥90
CAPEml	0.041	0.127	0.132	0.127	0.182	0.306	0.126	0.290	0.272	264.225	443.898	443.898	443.898	968.825	1032.239	443.898	1028.716	1028.716
CAPE03ml	0.046	0.093	0.092	0.096	0.177	0.187	0.091	−0.174	−0.174	58.830	67.525	67.525	67.525	37.370	40.330	67.525	81.400	81.400
CINml	0.043	−0.061	−0.048	−0.056	−0.114	−0.236	−0.061	−0.195	−0.190	9.701	57.365	57.365	57.365	56.802	64.254	57.365	64.254	64.254
LCLml	−0.124	−0.188	−0.197	−0.187	−0.194	−0.307	−0.180	−0.164	−0.166	663.408	732.784	732.784	732.784	862.864	656.904	730.616	520.320	520.320
CAPEmu	0.041	0.135	0.137	0.136	0.152	0.351	0.134	0.331	0.317	386.282	651.560	679.484	651.560	637.598	1265.888	651.560	1517.204	1265.888
WSSFC	0.104	0.180	0.180	0.171	0.250	**0.473**	0.173	0.306	0.312	3.210	3.630	3.620	3.620	3.100	3.750	3.630	3.750	3.750
WS500	0.255	0.364	0.353	0.358	**0.407**	***0.738***	0.346	**0.548**	**0.554**	13.536	13.280	14.656	13.280	13.792	18.304	13.280	19.584	19.648
WS1000	0.285	0.388	0.370	0.383	**0.494**	***0.717***	0.369	**0.453**	**0.460**	15.888	16.207	16.207	16.207	17.242	19.791	16.207	24.728	24.728
WS4000	0.322	**0.467**	**0.448**	**0.462**	**0.559**	***0.800***	**0.445**	**0.426**	**0.412**	22.635	23.104	23.104	23.104	23.104	27.472	23.104	27.472	27.472
WS6000	0.306	**0.460**	**0.444**	**0.453**	**0.529**	***0.707***	**0.440**	0.278	0.269	24.147	27.477	26.853	27.477	26.436	28.362	27.477	28.310	28.310
WS9000	0.265	**0.419**	0.399	**0.412**	**0.531**	***0.632***	**0.401**	0.260	0.246	31.095	30.408	30.283	30.283	31.720	30.471	30.283	34.342	37.839
WSLLmax	0.302	**0.405**	0.389	0.399	**0.501**	***0.731***	0.384	**0.430**	**0.433**	18.045	19.481	19.419	19.481	19.044	24.601	19.481	24.601	24.601
WSULmax	0.276	**0.426**	**0.406**	**0.420**	**0.533**	***0.646***	**0.407**	0.251	0.236	31.331	31.714	31.777	31.714	31.012	32.288	31.714	34.011	34.011
SRWSSFC	0.298	**0.434**	**0.418**	**0.430**	**0.532**	***0.626***	**0.414**	0.308	0.295	15.957	17.009	17.437	17.437	19.543	20.694	17.437	20.694	20.694
SRWS6000	0.071	0.105	0.115	0.109	0.118	−0.177	0.100	−0.268	-0.269	9.635	9.763	9.763	9.763	10.912	11.358	9.763	10.784	10.784
BWD500	0.260	0.357	0.347	0.351	**0.405**	***0.758***	0.339	**0.495**	**0.501**	10.333	10.309	10.309	10.309	9.910	13.670	10.309	13.670	13.670
BWD1000	0.271	0.360	0.344	0.352	**0.451**	***0.665***	0.343	0.339	0.327	12.335	15.443	15.443	15.443	13.065	16.489	15.443	16.331	16.331
BWD4000	0.297	**0.432**	**0.414**	**0.428**	**0.540**	***0.639***	**0.413**	0.306	0.298	20.048	22.646	22.646	22.646	21.656	24.668	22.646	29.453	29.453
BWD6000	0.286	**0.425**	**0.413**	**0.419**	**0.489**	***0.634***	**0.405**	0.231	0.224	24.223	24.223	24.223	25.603	26.603	25.032	24.223	25.032	25.032
BWD9000	0.240	0.378	0.358	0.373	**0.506**	**0.551**	0.361	0.234	0.221	27.933	28.295	28.234	28.295	29.200	27.028	28.295	34.328	34.388
BWDLLmax	0.288	0.385	0.371	0.379	**0.456**	***0.640***	0.365	0.312	0.312	15.423	17.233	16.984	17.233	15.298	18.982	17.233	22.541	22.541
BWDULmax	0.248	0.379	0.356	0.374	**0.511**	**0.562**	0.362	0.216	0.197	28.235	28.352	28.352	28.352	29.233	28.763	28.352	28.763	28.763
SRH500	0.284	**0.403**	0.399	**0.400**	**0.452**	***0.614***	0.383	0.281	0.271	140.230	137.837	134.008	137.837	127.308	185.218	137.837	185.218	185.218
SRH1000	0.277	0.384	0.376	0.380	**0.475**	**0.556**	0.365	0.256	0.247	180.244	184.148	184.148	184.148	169.833	197.162	184.148	261.581	261.581
SRH3000	0.266	0.355	0.345	0.355	**0.439**	**0.494**	0.337	0.260	0.255	244.559	238.248	238.248	238.248	214.581	310.827	238.248	354.216	354.216
SRMLIKE500	0.246	0.331	0.322	0.332	**0.426**	**0.467**	0.315	0.151	0.147	216.512	256.431	256.431	256.431	246.959	195.537	256.431	193.508	193.508
CA500	−0.211	−0.310	−0.288	−0.305	**−0.432**	***−0.610***	−0.296	−0.390	−0.375	70.920	69.120	69.120	69.120	69.840	56.880	69.120	44.820	44.820
STPcin500	0.242	0.361	0.355	0.355	**0.419**	***0.658***	0.347	0.396	0.380	0.931	1.387	1.387	1.387	0.873	2.221	1.387	3.113	3.123
VTPcin500	0.191	0.302	0.287	0.294	0.373	**0.571**	0.290	0.312	0.300	0.786	1.258	1.258	1.258	0.609	1.514	1.258	2.693	2.693
EHI500	0.237	0.366	0.362	0.361	**0.437**	***0.621***	0.353	0.361	0.347	0.438	0.758	0.758	0.758	0.443	1.067	0.758	1.732	1.752
LTTP	0.320	**0.466**	**0.442**	**0.459**	**0.572**	***0.760***	**0.445**	0.355	0.340	4.595	9.189	9.189	9.189	9.189	33.694	9.189	33.694	33.694
LTTPt	0.019	0.178	0.178	0.175	0.230	0.452	0.174	0.394	0.376	0.962	1.396	1.396	1.396	3.525	3.118	1.396	3.190	3.109
LTTPk	0.323	**0.465**	**0.451**	**0.457**	**0.551**	***0.746***	**0.444**	0.377	0.377	81.240	243.720	243.720	243.720	487.441	908.412	324.961	909.412	908.412

REFERENCES

Adlerman, E. J., K. K. Droegemeier, and R. Davies-Jones, 1999: A numerical simulation of cyclic mesocyclogenesis. *J. Atmos. Sci.*, **56**, 2045–2069, https://doi.org/10.1175/1520-0469(1999)056<2045:ANSOCM>2.0.CO;2.

Allouche, O., A. Tsoar, and R. Kadmon, 2006: Assessing the accuracy of species distribution models: Prevalence, kappa and the true skill statistic (TSS). *J. Appl. Ecol.*, **43**, 1223–1232, https://doi.org/10.1111/j.1365-2664.2006.01214.x.

Beebe, R. G., 1958: Tornado proximity soundings. *Bull. Amer. Meteor. Soc.*, **39**, 195–201, https://doi.org/10.1175/1520-0477-39.4.195.

Blumberg, W. G., K. T. Halbert, T. A. Supinie, P. T. Marsh, R. L. Thompson, and J. A. Hart, 2017: SHARPpy: An open-source sounding analysis toolkit for the atmospheric sciences. *Bull. Amer. Meteor. Soc.*, **98**, 1625–1636, https://doi.org/10.1175/BAMS-D-15-00309.1.

Britt, K. C., P. S. Skinner, P. L. Heinselman, and K. H. Knopfmeier, 2020: Effects of horizontal grid spacing and inflow environment on forecasts of cyclic mesocyclogenesis in NSSL's Warn-on-Forecast System (WoFS). *Wea. Forecasting*, **35**, 2423–2444, https://doi.org/10.1175/WAF-D-20-0094.1.

Brooks, H. E., C. A. Doswell III, and J. Cooper, 1994: On the environments of tornadic and nontornadic mesocyclones. *Wea. Forecasting*, **9**, 606–618, https://doi.org/10.1175/1520-0434(1994)009<0606:OTEOTA>2.0.CO;2.

——, J. W. Lee, and J. P. Craven, 2003: The spatial distribution of severe thunderstorm and tornado environments from global reanalysis data. *Atmos. Res.*, **67–68**, 73–94, https://doi.org/10.1016/S0169-8095(03)00045-0.

——, A. R. Anderson, K. Riemann, I. Ebbers, and H. Flachs, 2007: Climatological aspects of convective parameters from the NCAR/NCEP reanalysis. *Atmos. Res.*, **83**, 294–305, https://doi.org/10.1016/j.atmosres.2005.08.005.

Bryan, G. H., and J. M. Fritsch, 2004: A reevaluation of ice–liquid potential temperature. *Mon. Wea. Rev.*, **132**, 2421–2431, https://doi.org/10.1175/1520-0493(2004)132<2421:AROIWP>2.0.CO;2.

Bunkers, M. J., B. A. Klimowski, J. W. Zeitler, R. L. Thompson, and M. L. Weisman, 2000: Predicting supercell motion using a new hodograph technique. *Wea. Forecasting*, **15**, 61–79, https://doi.org/10.1175/1520-0434(2000)015<0061:PSMUAN>2.0.CO;2.

——, J. S. Johnson, L. J. Czepyha, J. M. Grzywacz, B. A. Klimowski, and M. R. Hjelmfelt, 2006: An observational examination of long-lived supercells. Part II: Environmental conditions and forecasting. *Wea. Forecasting*, **21**, 689–714, https://doi.org/10.1175/WAF952.1.

——, D. Barber, R. L. Thompson, R. Edwards, and J. Garner, 2014: Choosing a universal mean wind for supercell motion prediction. *J. Oper. Meteor.*, **2**, 115–129, https://doi.org/10.15191/nwajom.2014.0211.

Coffer, B. E., and M. D. Parker, 2018: Is there a "tipping point" between simulated nontornadic and tornadic supercells in VORTEX2 environments? *Mon. Wea. Rev.*, **146**, 2667–2693, https://doi.org/10.1175/MWR-D-18-0050.1.

——, ——, R. L. Thompson, B. T. Smith, and R. E. Jewell, 2019: Using near-ground storm relative helicity in supercell tornado forecasting. *Wea. Forecasting*, **34**, 1417–1435, https://doi.org/10.1175/WAF-D-19-0115.1.

——, M. Taszarek, and M. D. Parker, 2020: Near-ground wind profiles of tornadic and nontornadic environments in the United States and Europe from ERA5 reanalyses. *Wea. Forecasting*, **35**, 2621–2638, https://doi.org/10.1175/WAF-D-20-0153.1.

Cohen, J., 1988: *Statistical Power Analysis for the Behavioral Sciences*. Lawrence Erlbaum Associates, 567 pp.

Coniglio, M. C., 2012: Verification of RUC 0–1-h forecasts and SPC mesoscale analyses using VORTEX2 soundings. *Wea. Forecasting*, **27**, 667–683, https://doi.org/10.1175/WAF-D-11-00096.1.

——, and M. D. Parker, 2020: Insights into supercells and their environments from three decades of targeted radiosonde observations. *Mon. Wea. Rev.*, **148**, 4893–4915, https://doi.org/10.1175/MWR-D-20-0105.1.

——, and R. E. Jewell, 2022: SPC mesoscale analysis compared to field-project soundings: Implications for supercell environment studies. *Mon. Wea. Rev.*, **150**, 567–588, https://doi.org/10.1175/MWR-D-21-0222.1.

Cotton, W. R., G. H. Bryan, and S. C. van den Heever, 2010: *Storm and Cloud Dynamics*. 2nd ed. Academic Press, 820 pp.

Darkow, G. L., 1969: An analysis of over sixty tornado proximity soundings. *Sixth Conf. Severe Local Storms*, Chicago, IL, Amer. Meteor. Soc., 218–221.

Davenport, C. E., 2021: Environmental evolution of long-lived supercell thunderstorms in the Great Plains. *Wea. Forecasting*, **36**, 2187–2209, https://doi.org/10.1175/WAF-D-21-0042.1.

Davies, J. M., 2004: Estimations of CIN and LFC associated with tornadic and nontornadic supercells. *Wea. Forecasting*, **19**, 714–726, https://doi.org/10.1175/1520-0434(2004)019<0714:EOCALA>2.0.CO;2.

——, and R. H. Johns, 1993: Some wind and instability parameters associated with strong and violent tornadoes: 1. Wind shear and helicity. *The Tornado: Its Structure, Dynamics, Prediction, and Hazards*, *Geophys. Monogr.*, Vol. 79, Amer. Geophys. Union, 573–582.

Davies-Jones, R., D. Burgess, and M. Foster, 1990: Test of helicity as a tornado forecast parameter. *16th Conf. on Severe Local Storms*, Kananaskis, Alberta, Canada, Amer. Meteor. Soc., 588–592.

Doswell, C. A., III, and D. W. Burgess, 1988: On some issues of United States tornado climatology. *Mon. Wea. Rev.*, **116**, 495–501, https://doi.org/10.1175/1520-0493(1988)116<0495:OSIOUS>2.0.CO;2.

——, and E. N. Rasmussen, 1994: The effect of neglecting the virtual temperature correction on CAPE calculations. *Wea. Forecasting*, **9**, 625–629, https://doi.org/10.1175/1520-0434(1994)009<0625:TEONTV>2.0.CO;2.

——, and D. M. Schultz, 2006: On the use of indices and parameters in forecasting severe storms. *Electron. J. Severe Storms Meteor.*, **1** (3), https://ejssm.com/ojs/index.php/site/article/view/4/3.

——, R. Davies-Jones, and D. L. Keller, 1990: On summary measures of skill in rare event forecasting based on contingency tables. *Wea. Forecasting*, **5**, 576–585, https://doi.org/10.1175/1520-0434(1990)005<0576:OSMOSI>2.0.CO;2.

Dowell, D. C., and H. B. Bluestein, 2002: The 8 June 1995 McLean, Texas, storm. Part II: Cyclic tornado formation, maintenance, and dissipation. *Mon. Wea. Rev.*, **130**, 2649–2670, https://doi.org/10.1175/1520-0493(2002)130<2649:TJMTSP>2.0.CO;2.

Edwards, R., H. E. Brooks, and H. Cohn, 2021: Changes in tornado climatology accompanying the enhanced Fujita scale. *J. Appl. Meteor. Climatol.*, **60**, 1465–1482, https://doi.org/10.1175/JAMC-D-21-0058.1.

Esterheld, J. M., and D. J. Giuliano, 2008: Discriminating between tornadic and non-tornadic supercells: A new hodograph technique. *Electron. J. Severe Storms Meteor.*, **3** (2), https://ejssm.com/ojs/index.php/site/article/view/15.

Evans, J. S., and C. A. Doswell III, 2001: Examination of derecho environments using proximity soundings. *Wea. Forecasting*, **16**, 329–342, https://doi.org/10.1175/1520-0434(2001)016<0329:EODEUP>2.0.CO;2.

Garner, J. M., 2007: A preliminary study on environmental parameters related to tornado path length. *Electron. J. Oper. Meteor.*, Electron. J. Oper. Meteor., 2007-EJ5, http://nwafiles.nwas.org/ej/pdf/2007-EJ5.pdf.

——, W. C. Iwasko, T. D. Jewel, R. L. Thompson, and B. T. Smith, 2021: An environmental study on tornado pathlength, longevity, and width. *Wea. Forecasting*, **36**, 1471–1490, https://doi.org/10.1175/WAF-D-20-0230.1.

Gensini, V. A., and W. S. Ashley, 2011: Climatology of potentially severe convective environments from the North American regional reanalysis. *Electron. J. Severe Storms Meteor.*, **6** (8), https://ejssm.com/ojs/index.php/site/article/view/35/35.

——, T. L. Mote, and H. E. Brooks, 2014: Severe-thunderstorm reanalysis environments and collocated radiosonde observations. *J. Appl. Meteor. Climatol.*, **53**, 742–751, https://doi.org/10.1175/JAMC-D-13-0263.1.

——, C. Converse, W. S. Ashley, and M. Taszarek, 2021: Machine learning classification of significant tornadoes and hail in the United States using ERA5 proximity soundings. *Wea. Forecasting*, **36**, 2143–2160, https://doi.org/10.1175/WAF-D-21-0056.1.

Grazulis, T. P., 2023: *Significant Tornadoes 1974-2022*. The Tornado Project, 684 pp.

Grieser, J., and F. Terenzi, 2016: Modeling financial losses resulting from tornadoes in European countries. *Wea. Climate Soc.*, **8**, 313–326, https://doi.org/10.1175/WCAS-D-15-0036.1.

Hampshire, N. L., R. M. Mosier, T. M. Ryan, and D. E. Cavanaugh, 2018: Relationship of low-level instability and tornado damage rating based on observed soundings. *J. Oper. Meteor.*, **6** (1), 1–12, https://doi.org/10.15191/nwajom.2018.0601.

Hart, J. A., and W. Korotky, 1991: The SHARP workstation v1.50 users guide. NOAA National Weather Service Doc., 30 pp.

Hersbach, H., and Coauthors, 2020: The ERA5 global reanalysis. *Quart. J. Roy. Meteor. Soc.*, **146**, 1999–2049, https://doi.org/10.1002/qj.3803.

Hill, A. J., G. R. Herman, and R. S. Schumacher, 2020: Forecasting severe weather with random forests. *Mon. Wea. Rev.*, **148**, 2135–2161, https://doi.org/10.1175/MWR-D-19-0344.1.

Johns, R. H., J. M. Davies, and P. W. Leftwich, 1993: Some wind and instability parameters associated with strong and violent tornadoes: 2. Variations in the combinations of wind and instability parameters. *The Tornado: Its Structure, Dynamics, Prediction, and Hazards*, *Geophys. Monogr.*, Vol. 79, Amer. Geophys. Union, 583–590.

Kasuya, E., 2001: Mann–Whitney *U* test when variances are unequal. *Anim. Behav.*, **61**, 1247–1249, https://doi.org/10.1006/anbe.2001.1691.

Kelly, D. L., J. T. Schaefer, R. P. McNulty, C. A. Doswell III, and R. F. Abbey Jr., 1978: An augmented tornado climatology. *Mon. Wea. Rev.*, **106**, 1172–1183, https://doi.org/10.1175/1520-0493(1978)106<1172:AATC>2.0.CO;2.

King, A. T., and A. D. Kennedy, 2019: North American supercell environments in atmospheric reanalyses and RUC-2. *J. Appl. Meteor. Climatol.*, **58**, 71–92, https://doi.org/10.1175/JAMC-D-18-0015.1.

Komac, B., P. Esteban, L. Trapero, and R. Caritg, 2016: Modelization of the current and future habitat suitability of *Rhododendron ferrugineum* using potential snow accumulation. *PLOS ONE*, **11**, e0147324, https://doi.org/10.1371/journal.pone.0147324.

Mann, H. B., and D. R. Whitney, 1947: On a test of whether one of two random variables is stochastically larger than the other. *Ann. Math. Stat.*, **18**, 50–60, https://doi.org/10.1214/aoms/1177730491.

Markowski, P. M., E. N. Rasmussen, and J. M. Straka, 1998a: The occurrence of tornadoes in supercells interacting with boundaries during VORTEX-95. *Wea. Forecasting*, **13**, 852–859, https://doi.org/10.1175/1520-0434(1998)013<0852:TOOTIS>2.0.CO;2.

——, ——, ——, and D. C. Dowell, 1998b: Observations of low-level baroclinity generated by anvil shadows. *Mon. Wea. Rev.*, **126**, 2942–2958, https://doi.org/10.1175/1520-0493(1998)126<2942:OOLLBG>2.0.CO;2.

——, J. M. Straka, E. N. Rasmussen, and D. O. Blanchard, 1998c: Variability of storm-relative helicity during VORTEX. *Mon. Wea. Rev.*, **126**, 2959–2971, https://doi.org/10.1175/1520-0493(1998)126<2959:VOSRHD>2.0.CO;2.

——, C. Hannon, J. Frame, E. Lancaster, A. Pietrycha, R. Edwards, and R. L. Thompson, 2003: Characteristics of vertical wind profiles near supercells obtained from the rapid update cycle. *Wea. Forecasting*, **18**, 1262–1272, https://doi.org/10.1175/1520-0434(2003)018<1262:COVWPN>2.0.CO;2.

Marquis, J., Y. Richardson, P. Markowski, D. Dowell, and J. Wurman, 2012: Tornado maintenance investigated with high-resolution dual-Doppler and EnKF analysis. *Mon. Wea. Rev.*, **140**, 3–27, https://doi.org/10.1175/MWR-D-11-00025.1.

Murdzek, S. S., Y. P. Richardson, and P. M. Markowski, 2024: The sensitivity of supercell cold pools to the lifting condensation level and the predicted particle properties microphysics scheme. *Mon. Wea. Rev.*, **152**, 1179–1200, https://doi.org/10.1175/MWR-D-23-0092.1.

Nachar, N., 2008: The Mann-Whitney U: A test for assessing whether two independent samples come from the same distribution. *Tutorials Quant. Methods Psychol.*, **4**, 13–20, https://doi.org/10.20982/tqmp.04.1.p013.

Nixon, C. J., and J. T. Allen, 2022: Distinguishing between hodographs of severe hail and tornadoes. *Wea. Forecasting*, **37**, 1761–1782, https://doi.org/10.1175/WAF-D-21-0136.1.

NOAA-NWS, 2013: May 28th, 2013 Ottawa County EF-3 Tornado. National Oceanic and Atmospheric Administration, National Weather Service Office, https://www.weather.gov/top/2013_OttawaTor#:~:text=The%20tornado%20was%20on%20the,head%20of%20cattle%20were%20lost.

Parker, M. D., 2014: Composite VORTEX2 supercell environments from near-storm soundings. *Mon. Wea. Rev.*, **142**, 508–529, https://doi.org/10.1175/MWR-D-13-00167.1.

Peters, J. M., B. E. Coffer, M. D. Parker, C. J. Nowotarski, J. P. Mulholland, C. J. Nixon, and J. T. Allen, 2023: Disentangling the influences of storm-relative flow and horizontal streamwise vorticity on low-level mesocyclones in supercells. *J. Atmos. Sci.*, **80**, 129–149, https://doi.org/10.1175/JAS-D-22-0114.1.

Potvin, C. K., K. L. Elmore, and S. J. Weiss, 2010: Assessing the impacts of proximity sounding criteria on the climatology of significant tornado environments. *Wea. Forecasting*, **25**, 921–930, https://doi.org/10.1175/2010WAF2222368.1.

Rasmussen, E. N., 2003: Refined supercell and tornado forecast parameters. *Wea. Forecasting*, **18**, 530–535, https://doi.org/10.1175/1520-0434(2003)18<530:RSATFP>2.0.CO;2.

——, and D. O. Blanchard, 1998: A baseline climatology of sounding-derived supercell and tornado forecast parameters. *Wea. Forecasting*, **13**, 1148–1164, https://doi.org/10.1175/1520-0434(1998)013<1148:ABCOSD>2.0.CO;2.

——, and J. M. Straka, 1998: Variations in supercell morphology. Part I: Observations of the role of upper-level storm-relative flow. *Mon. Wea. Rev.*, **126**, 2406–2421, https://doi.org/10.1175/1520-0493(1998)126<2406:VISMPI>2.0.CO;2.

——, S. Richardson, J. M. Straka, P. M. Markowski, and D. O. Blanchard, 2000: The association of significant tornadoes with a baroclinic boundary on 2 June 1995. *Mon. Wea. Rev.*, **128**, 174–191, https://doi.org/10.1175/1520-0493(2000)128<0174:TAOSTW>2.0.CO;2.

Schaefer, J. T., and R. L. Livingston, 1988: The typical structure of tornado proximity soundings. *J. Geophys. Res.*, **93**, 5351–5364, https://doi.org/10.1029/JD093iD05p05351.

——, and R. Edwards, 1999: The SPC tornado/severe thunderstorm database. *11th Conf. Applied Climatology*, Dallas, TX, Amer. Meteor. Soc., 215–220, https://www.spc.noaa.gov/publications/schaefer/database.htm.

Sherburn, K. D., and M. D. Parker, 2014: Climatology and ingredients of significant severe convection in high-shear, low-CAPE environments. *Wea. Forecasting*, **29**, 854–877, https://doi.org/10.1175/WAF-D-13-00041.1.

Straka, J., and K. Kanak, 2022: A climatology of long-track tornadoes. *Electron. J. Severe Storms Meteor.*, **17** (1), https://ejssm.com/ojs/index.php/site/article/view/82.

Taszarek, M., J. T. Allen, P. Groenemeijer, R. Edwards, H. E. Brooks, V. Chmielewski, and S.-E. Enno, 2020a: Severe convective storms across Europe and the United States. Part I: Climatology of lightning, large hail, severe wind, and tornadoes. *J. Climate*, **33**, 10 239–10 261, https://doi.org/10.1175/JCLI-D-20-0345.1.

——, ——, T. Púčik, K. A. Hoogewind, and H. E. Brooks, 2020b: Severe convective storms across Europe and the United States. Part II: ERA5 environments associated with lightning, large hail, severe wind, and tornadoes. *J. Climate*, **33**, 10 263–10 286, https://doi.org/10.1175/JCLI-D-20-0346.1.

Thompson, R. L., 1998: Eta Model storm-relative winds associated with tornadic and nontornadic supercells. *Wea. Forecasting*, **13**, 125–137, https://doi.org/10.1175/1520-0434(1998)013<0125:EMSRWA>2.0.CO;2.

——, R. Edwards, J. A. Hart, K. L. Elmore, and P. Markowski, 2003: Close proximity soundings within supercell environments obtained from the rapid update cycle. *Wea. Forecasting*, **18**, 1243–1261, https://doi.org/10.1175/1520-0434(2003)018<1243:CPSWSE>2.0.CO;2.

——, C. M. Mead, and R. Edwards, 2007: Effective storm-relative helicity and bulk shear in supercell thunderstorm environments. *Wea. Forecasting*, **22**, 102–115, https://doi.org/10.1175/WAF969.1.

Verbout, S. M., H. E. Brooks, L. M. Leslie, and D. M. Schultz, 2006: Evolution of the U.S. tornado database: 1954–2003. *Wea. Forecasting*, **21**, 86–93, https://doi.org/10.1175/WAF910.1.

Weisman, M. L., and J. B. Klemp, 1982: The dependence of numerically simulated convective storms on vertical wind shear and buoyancy. *Mon. Wea. Rev.*, **110**, 504–520, https://doi.org/10.1175/1520-0493(1982)110<0504:TDONSC>2.0.CO;2.

——, and ——, 1984: The structure and classification of numerically simulated convective storms in directionally varying wind shears. *Mon. Wea. Rev.*, **112**, 2479–2498, https://doi.org/10.1175/1520-0493(1984)112<2479:TSACON>2.0.CO;2.

Welch, B. L., 1947: The generalization of 'Student's' problem when several different population variances are involved. *Biometrika*, **34**, 28–35, https://doi.org/10.2307/2332510.

Wilcox, R. R., 2023: A heteroscedastic analog of the Wilcoxon–Mann–Whitney test when there is a covariate. *Int. J. Stat. Probab.*, **12**, 18–27, https://doi.org/10.5539/ijsp.v12n2p18.

Wurman, J., K. Kosiba, T. White, and P. Robinson, 2021: Supercell tornadoes are much stronger and wider than damage-based ratings indicate. *Proc. Natl. Acad. Sci. USA*, **118**, e2021535118, https://doi.org/10.1073/pnas.2021535118.